

Systematic parametrization of the leading B -meson light-cone distribution amplitude

Thorsten Feldmann,^a Philip Lüghausen^{b,c} and Danny van Dyk^c

^a*Theoretische Physik 1, Universität Siegen,
Walter-Flex-Straße 3, D-57068 Siegen, Germany*

^b*Excellence Cluster ORIGINS, Technische Universität München,
Boltzmannstraße 2, D-85748 Garching, Germany*

^c*Physik Department T31, Technische Universität München,
James-Franck-Straße 1, D-85748 Garching, Germany*

E-mail: thorsten.feldmann@uni-siegen.de, philip.lueghausen@tum.de,
danny.van.dyk@gmail.com

ABSTRACT: We propose a parametrization of the leading B -meson light-cone distribution amplitude (LCDA) in heavy-quark effective theory (HQET). In position space, it uses a conformal transformation that yields a systematic Taylor expansion and an integral bound, which enables control of the truncation error. Our parametrization further produces compact analytical expressions for a variety of derived quantities. At a given reference scale, our momentum-space parametrization corresponds to an expansion in associated Laguerre polynomials, which turn into confluent hypergeometric functions ${}_1F_1$ under renormalization-group evolution at one-loop accuracy. Our approach thus allows a straightforward and transparent implementation of a variety of phenomenological constraints, regardless of their origin. Moreover, we can include theoretical information on the Taylor coefficients by using the local operator product expansion. We showcase the versatility of the parametrization in a series of phenomenological pseudo-fits.

KEYWORDS: Bottom Quarks, Effective Field Theories of QCD

ARXIV EPRINT: [2203.15679](https://arxiv.org/abs/2203.15679)

Contents

1	Introduction	1
2	Prerequisites	3
2.1	Mathematical properties	3
2.2	Renormalization and eigenfunctions	4
2.3	Logarithmic moments and generating function	5
2.4	Behavior at small momentum	7
3	Parametrization of the B-meson LCDA	7
3.1	LCDA in dual space and logarithmic moments	10
3.2	Momentum-space LCDA and behavior at $\omega = 0$	12
3.3	RG evolution	13
3.4	Application to higher twist	15
4	Application to existing models	16
4.1	Exponential model	18
4.2	Lee-Neubert model with radiative tail	20
4.3	Naïve parton model	23
4.4	A model with $\phi'_+(0) \rightarrow \infty$	25
5	Pseudo-phenomenology	27
5.1	Using λ_B and ℓ_5 as phenomenological constraints	27
5.1.1	Exponential model	29
5.1.2	Lee-Neubert model with radiative tail	30
5.1.3	Naïve parton model	30
5.1.4	Model with $\phi'_+(0) \rightarrow \infty$	30
5.2	Adding theoretical constraints from the short-distance OPE	31
6	Conclusion and outlook	34
A	Useful definitions and formulas	36
B	Solutions for expansion coefficients a_k from pseudo-phenomenology and OPE	37

1 Introduction

Light-cone distribution amplitudes (LCDA) of the B -meson are needed as hadronic input functions for the theoretical descriptions of exclusive (energetic) B -meson decays. These descriptions include factorization theorems in Quantum Chromodynamics (QCD), which have first been introduced to tackle charmless non-leptonic B -decays [1, 2]. They have later also been applied to other decay modes, including semi-leptonic and radiative decays (see e.g. the corresponding chapter in [3] for a recent overview and an exhaustive list of references). The descriptions further include light-cone sum rules (LCSR), which are a complementary approach. These sum rules can be used to determine “soft” hadronic matrix elements for which the factorization of the initial and final states does not work completely. A formulation of light-cone sum rules with B -meson LCDA has been proposed in refs. [4–7]. It has the advantage that the very same hadronic input functions appear as in QCD factorization. This fact has recently been exploited to show that precise theoretical predictions for the benchmark decay mode $B \rightarrow \gamma \ell \nu$ can be obtained [8–10], which in turn allows inferring the relevant information on the B -meson LCDA from future experimental data, notably from the Belle-2 experiment; see the corresponding paragraph in ref. [3].

The leading B -meson LCDA enters the aforementioned theoretical approaches in different ways:

1. The leading-power terms in QCD factorization involve logarithmic moments of the B -meson LCDA. The definition of these logarithmic moments follows later.
2. In LCSR the B -meson LCDA enters in the form of integrals where the contributions from large light-cone momenta are parametrically suppressed. We later define appropriate quantities to describe the low-momentum behavior of the B -meson LCDA relevant for these sum-rule applications.

Adhoc models of the LCDA introduce non-trivial and potentially unphysical correlations within and between these two sets of quantities. The modelling itself and together with these correlations give rise to unquantifiable systematic uncertainties in the determination of the leading-twist LCDA, e.g., from the photoleptonic decay $\bar{B} \rightarrow \gamma \ell^- \bar{\nu}$. One of the main results of this work is a parametrization of the LCDA that is general enough to avoid unjustified correlations between its observable features and that includes as much model-independent theoretical information as possible.

Parametrizing the soft contribution of the B -meson LCDA introduces by definition a low reference momentum scale (in the following denoted as ω_0), which characterizes hadronic dynamics. In previously discussed benchmark models, this scale has often been identified with the HQET parameter $\bar{\Lambda}$ by using theoretical expressions for the positive moments of the LCDA, either at tree level [11] or including the radiative tail [12]. Our parametrization for the LCDA starts from an infinite series of terms, such that the moment constraints can be fulfilled at each order of the HQET expansion for any value of ω_0 . The only constraint on this otherwise free parameter is coming from the requirement that the expansion coefficients are sufficiently converging, which again forces ω_0 to be *of the*

same order as $\bar{\Lambda}$. In practice, we can truncate the expansion after a few terms, and the intrinsic uncertainty of the truncation can be estimated by varying the parameter ω_0 in a reasonable range.

The theoretical properties of B -meson LCDAs have been studied extensively in the past. For the scope of this work, two related aspects turn out to be most important:

- the behavior of LCDAs under change of the renormalization scale; and
- the behavior of LCDAs at large light-cone momentum of the light quark (i.e. at short separations of the fields in the defining light-cone operator).

In both cases, one has to carefully study the renormalization of light-cone operators in the heavy-quark limit, i.e. the treatment of the b -quark as a static source of color in heavy-quark effective theory (HQET). The resulting renormalization group (RG) equation for the B -meson LCDA has been first calculated at the one-loop level by Lange and Neubert [13]. The eigenfunctions of the one-loop RG kernel have first been identified in ref. [14], which shortly thereafter have been reproduced from conformal symmetry considerations [15]. The latter method has very recently been used to derive the RG kernel for the B -meson LCDA at two loops [16], and the solution of the RG equation and its implementation into QCD factorization theorems have been discussed in refs. [17, 18]. Here we will restrict ourselves to one-loop accuracy. However, our formalism is general enough to allow the implementation of two-loop effects.

This article is structured as follows. We summarize the properties of the leading B -meson LCDA ϕ_+ and define our notations in section 2. This includes a brief discussion of the relevant analytic properties, the renormalization at one-loop level, the generating function for the logarithmic moments, and the definition of suitable quantities to describe the low-momentum behavior. In section 3 we introduce our novel parametrization for the B -meson LCDA $\tilde{\phi}_+(\tau)$ in position space. Starting from a conformal transformation $\tau \mapsto y$, which maps the real τ axis onto the unit circle in the complex y -plane, we construct a Taylor expansion in the variable y , where the Taylor coefficients are constrained by an integral bound. We translate our parametrization to the so-called “dual” space and to momentum space. In both cases, this results in an expansion in terms of associated Laguerre polynomials. We also provide expressions for the logarithmic moments and discuss different options to implement the effect of the RG evolution. Moreover, we briefly discuss how to generalize our formalism to higher-twist LCDAs, restricting ourselves to the Wandzura-Wilczek limit. Our parametrization is generic enough to capture the features of a variety of benchmark models discussed in the literature. This is illustrated in section 4 where we study the convergence properties of our expansion for four examples of such models. To set the stage for future phenomenological applications, in section 5, we perform numerical fits on the basis of two pseudo-observables that are expected to be well constrained by future data on the photo-leptonic $B \rightarrow \gamma \ell \nu$ decay. In addition, we show how including theoretical information from the local operator product expansion (OPE) yields further constraints of the expansion coefficients in phenomenological fits. We conclude in section 6 and provide some additional formulas in two appendices.

2 Prerequisites

The leading-twist¹ LCDA of the B -meson is defined as the matrix element of a light-cone operator in HQET normalized to the matrix element of the corresponding local operator [11]:

$$\tilde{\phi}_+(\tau; \mu) = \frac{\langle 0 | \bar{q}(\tau n) [\tau n, 0] \not{n} \gamma_5 h_v(0) | B(v) \rangle}{\langle 0 | \bar{q}(0) \not{n} \gamma_5 h_v(0) | B(v) \rangle}. \quad (2.1)$$

Here n^μ is a light-like vector with $n^2 = 0$, and the gauge link $[\tau n, 0]$ appears as a straight Wilson line that renders the definition of $\tilde{\phi}_+(\tau)$ gauge invariant in QCD. The B -meson moves with velocity v^μ . For simplicity we are considering a frame with $v \cdot n = 1$. The limit $m_b \rightarrow \infty$ has already been taken in HQET. Hence, $\tilde{\phi}_+$ does not depend on the heavy-quark mass m_b . The m_b -dependence of physical amplitudes is contained in short-distance coefficient functions that multiply the LCDA, e.g., in QCD factorization calculations.

2.1 Mathematical properties

In position space, the LCDA fulfills the following three properties. They have previously been discussed, e.g., in ref. [20]:

P1: $\tilde{\phi}_+(\tau)$ is analytic in the lower complex half plane $\text{Im } \tau < 0$.

P2: $\tilde{\phi}_+(\tau)$ is analytic on the real τ axis, except for a single point $\tau = 0$ where it has a logarithmic singularity of measure zero, with a branch cut extending along the positive imaginary axis. Hence $\tilde{\phi}_+(\tau)$ is Lebesgue-integrable with

$$\lim_{\epsilon \rightarrow 0^+} \int_{-\infty - i\epsilon}^{\infty - i\epsilon} d\tau \tilde{\phi}_+(\tau, \mu) = 0 \quad (2.2)$$

P3: $\tilde{\phi}_+(\tau)$ can be analytically continued from the lower complex half plane onto the real τ axis *almost everywhere* (i.e. in all points except for a null set).

In the following we assume that the Fourier transform exists,

$$\phi_+(\omega; \mu) = \int_{-\infty - i\epsilon}^{+\infty - i\epsilon} \frac{d\tau}{2\pi} e^{i\omega\tau} \tilde{\phi}_+(\tau; \mu). \quad (2.3)$$

It follows from the properties **P1** to **P3** and the Paley-Wiener theorem [21, theorem 7.2.4] that $\tilde{\phi}_+(\tau)$ is the *holomorphic Fourier transform* of a function $\phi_+(\omega)$,

$$\tilde{\phi}_+(\tau; \mu) = \int_0^\infty d\omega e^{-i\omega\tau} \phi_+(\omega; \mu), \quad (2.4)$$

and that $\phi_+(\omega) \in L^2$ on the support $[0, \infty)$. Plancherel's theorem then provides that both $\tilde{\phi}_+(\tau)$ and $\phi_+(\omega)$ are square-integrable on the entire real τ axis and the positive ω axis, respectively, and their two-norms coincide:

$$\int_{-\infty}^{+\infty} \frac{d\tau}{2\pi} |\tilde{\phi}_+(\tau)|^2 = \int_0^\infty d\omega |\phi_+(\omega)|^2 < \infty. \quad (2.5)$$

As consequence, the inner product exists in both the ω space and the τ space.

¹The notion of twist has to be modified for the discussion of light-cone operators in HQET; see ref. [19].

We further assume that $\phi_+(\omega; \mu) \propto \omega$ for $\omega \rightarrow 0$ at large renormalization scales $\mu \gg \Lambda_{\text{had}}$. This is supported by the asymptotic behavior due to approximate conformal symmetry within the twist expansion [22]. From this assumed behavior at $\omega = 0$ one further property follows:

P4: The position space LCDA must asymptotically fall off at least as fast as $1/\tau^2$:

$$0 \leq \lim_{\tau \rightarrow \infty} \left| \tau^2 \tilde{\phi}(\tau) \right| < \infty. \quad (2.6)$$

In QCD factorization theorems, the momentum-space argument $\omega = n \cdot l$ represents the light-cone projection of the light spectator-quark momentum l^μ in the B -meson. We remark that the support of the matrix element in eq. (2.1) is different from the corresponding expressions for a light pseudoscalar meson, due to the different analytic properties of the heavy-quark propagator in HQET compared to a light-quark propagator in full QCD. As a consequence, $\omega \in [0, \infty)$.

2.2 Renormalization and eigenfunctions

The B -meson LCDA $\phi_+(\omega)$ can be expanded in terms of a *continuous* set of eigenfunctions of the one-loop renormalization-group (RG) equation, which can be expressed through Bessel functions of the first kind [14, 15]. Following the convention of ref. [15] one has²

$$\begin{aligned} \phi_+(\omega, \mu) &= \int_0^\infty ds \sqrt{\omega s} J_1(2\sqrt{\omega s}) \eta_+(s, \mu) \\ \Leftrightarrow s \eta_+(s; \mu) &= \int_0^\infty \frac{d\omega}{\omega} \sqrt{\omega s} J_1(2\sqrt{\omega s}) \phi_+(\omega; \mu). \end{aligned} \quad (2.7)$$

The notation for the function $\eta_+(s)$ is related to the function $\rho_+(\omega')$ as defined in ref. [14] via the relation

$$s \eta_+(s; \mu) = \rho_+(\omega' = 1/s; \mu). \quad (2.8)$$

In this work we use the notation of ref. [15]. For convenience we also quote the relation between the dual-space LCDA and the position-space LCDA, see also ref. [14],

$$\begin{aligned} s \eta_+(s; \mu) &= \int_{-\infty - i\epsilon}^{+\infty - i\epsilon} \frac{d\tau}{2\pi} \left(1 - e^{-is/\tau} \right) \tilde{\phi}_+(\tau; \mu) \\ \Leftrightarrow \tilde{\phi}_+(\tau; \mu) &= -\frac{1}{\tau^2} \int_0^\infty ds e^{\frac{is}{\tau}} s \eta_+(s; \mu). \end{aligned} \quad (2.9)$$

²The transformations in eq. (2.7) imply that the momentum-space LCDA $\phi_+(\omega, \mu)$ grows linearly in ω for small momenta, and its dual $\eta_+(s, \mu)$ goes to a constant at $s \rightarrow 0$.

The purpose of these integral transformations is to showcase that the function $\eta_+(s)$ obeys a simple multiplicative RG equation at one-loop,³

$$\frac{d\eta_+(s; \mu)}{d \ln \mu} = - \left[\Gamma_c(\alpha_s(\mu)) \ln \left(\mu s e^{2\gamma_E} \right) + \gamma_+(\alpha_s(\mu)) \right] \eta_+(s; \mu). \quad (2.10)$$

Its explicit solution reads

$$\eta_+(s; \mu) = e^{V(\mu; \mu_0)} \eta_+(s; \mu_0) (\hat{\mu}_0 s)^{-g(\mu; \mu_0)}. \quad (2.11)$$

Here and in the following, we use the short-hand notation

$$\hat{\mu} \equiv \mu e^{2\gamma_E}, \quad (2.12)$$

and similar for other quantities. Our definitions of the functions $V(\mu; \mu_0)$ and $g(\mu; \mu_0)$ coincide with the conventions used, e.g., in ref. [14]. They are given in eq. (A.1) and eq. (A.2) in the appendix, respectively. For convenience, we quote their RG equations:

$$\frac{dV(\mu, \mu_0)}{d \ln \mu} = - \left[\Gamma_c(\alpha_s(\mu)) \ln \left(\frac{\mu}{\mu_0} \right) + \gamma_+(\alpha_s(\mu)) \right], \quad \frac{dg(\mu, \mu_0)}{d \ln \mu} = \Gamma_c(\alpha_s(\mu)). \quad (2.13)$$

2.3 Logarithmic moments and generating function

In QCD factorization theorems for exclusive B -meson decays [1, 2] the B -meson LCDA enters in terms of logarithmic moments. It is convenient to define these moments directly from the spectral representation [14, 23]. In the following, we will use the convention

$$L_n(\mu, \mu_m) = (-1)^n \int_0^\infty ds \ln^n (\hat{\mu}_m s) \eta_+(s; \mu), \quad (2.14)$$

where L_0 is commonly called $1/\lambda_B$. We emphasize that in the definition of the logarithmic moments L_n with $n \geq 1$, we have considered a fixed reference momentum scale μ_m . Alternative definitions in the literature have used the renormalization scale μ itself or the zeroth logarithmic moment λ_B . The Mellin transform of $\eta_+(s)$

$$F_{[\eta_+]}(t; \mu, \mu_m) \equiv \int_0^\infty ds (\hat{\mu}_m s)^{-t} \eta_+(s; \mu) \quad (2.15)$$

conveniently generates the moments L_n as the coefficients of its Taylor expansion around $t = 0$:

$$L_n(\mu, \mu_m) = \left(\frac{d}{dt} \right)^n F_{[\eta_+]}(t; \mu, \mu_m) \Big|_{t=0}. \quad (2.16)$$

³Recently, the two-loop RG equation has been derived in ref. [16],

$$\left(\frac{d}{d \ln \mu} + \Gamma_c \ln(\hat{\mu} s) + \gamma_+ \right) \eta_+(s; \mu) = 4C_F \left(\frac{\alpha_s}{4\pi} \right)^2 \int_0^1 du \frac{\bar{u}}{u} h(u) \eta_+(\bar{u}s; \mu),$$

where $\bar{u} \equiv 1 - u$ and the function $h(u)$ is given by

$$h(u) = \ln \bar{u} \left[\beta_0 + 2C_F \left(\ln \bar{u} - \frac{1+\bar{u}}{\bar{u}} \ln u - \frac{3}{2} \right) \right], \quad \text{with } h(0) = 0.$$

We similarly define the generating function⁴ of the logarithmic moments of $\phi_+(\omega)$

$$G_{[\phi_+]}(t; \mu, \mu_m) = \int_0^\infty \frac{d\omega}{\omega} \left(\frac{\mu_m}{\omega} \right)^{-t} \phi_+(\omega, \mu), \quad (2.17)$$

which is related to the previous generating function by

$$G_{[\phi_+]}(t; \mu, \mu_m) = \frac{\Gamma(1+t)}{\Gamma(1-t)} e^{2\gamma_E t} F_{[\eta_+]}(t; \mu, \mu_m) = F_{[\eta_+]}(t; \mu, \mu_m) \left(1 + \mathcal{O}(t^3) \right) \quad (t < 1). \quad (2.18)$$

Evidently, the logarithmic moments of η_+ and ϕ_+ coincide for $n = 0, 1, 2$. We regularly omit the argument μ_m in the logarithmic moments and the generating functionals for brevity.

The logarithmic moments L_n obey simple coupled RG equations at one-loop (see also ref. [14]),

$$\frac{dL_n(\mu, \mu_m)}{d \ln \mu} = \Gamma_c(\mu) L_{n+1}(\mu, \mu_m) - \Gamma_c(\mu) \ln \frac{\mu}{\mu_m} L_n(\mu, \mu_m) - \gamma_+(\mu) L_n(\mu, \mu_m). \quad (2.19)$$

For the particular choice $\mu_m = \mu_0$ one obtains the simple solution

$$L_n(\mu, \mu_0) = e^{V(\mu, \mu_0)} \sum_{k=0}^{\infty} \frac{[g(\mu, \mu_0)]^k}{k!} L_{n+k}(\mu_0, \mu_0). \quad (2.20)$$

The result for an arbitrary choice of μ_m follows from

$$\begin{aligned} L_n(\mu, \mu_m) &= \sum_{i=0}^n \binom{n}{i} L_i(\mu, \mu_0) \left(\ln \frac{\mu_0}{\mu_m} \right)^{n-i} \\ &= e^{V(\mu, \mu_0)} \left(\frac{\mu_0}{\mu_m} \right)^{-g(\mu, \mu_0)} \sum_{k=0}^{\infty} \frac{[g(\mu, \mu_0)]^k}{k!} L_{n+k}(\mu_0, \mu_m). \end{aligned} \quad (2.21)$$

The generating function $F_{[\eta_+]}(t; \mu, \mu_m)$ is particularly useful, because it has a simple scale dependence that follows from eq. (2.11),

$$F_{[\eta_+]}(t; \mu, \mu_m) = e^{V(\mu; \mu_0)} \left(\frac{\mu_0}{\mu_m} \right)^{-g(\mu; \mu_0)} F_{[\eta_+]}(t + g(\mu; \mu_0); \mu_0, \mu_m) \quad (2.22)$$

This is the solution of the RG equation,

$$\frac{\partial F_{[\eta_+]}(t; \mu)}{\partial \ln \mu} = - \left(\gamma_+(\mu) + \Gamma_c(\mu) \ln \frac{\mu}{\mu_m} \right) F_{[\eta_+]}(t; \mu) + \Gamma_c(\mu) \frac{\partial F_{[\eta_+]}(t; \mu)}{\partial t} \quad (2.23)$$

The two-loop RG equation for $G_{[\phi_+]}$ and its solution can be found in ref. [18], which can easily be translated to $F_{[\eta_+]}$ via eq. (2.18).

Finally, we note that the generating function $F_{[\eta_+]}$ can directly be obtained from the position-space LCDA via

$$F_{[\eta_+]}(t; \mu, \mu_m) = \frac{\Gamma(1-t)}{t} \int_{-\infty}^{\infty} \frac{d\tau}{2\pi} \left(\frac{i}{\hat{\mu}_m \tau} \right)^t \tilde{\phi}_+(\tau; \mu). \quad (2.24)$$

⁴The function $G_{[\phi_+]}$ has also been used in the first analysis of the RG equation for $\phi_+(\omega; \mu)$ in ref. [13]. As has been shown in ref. [18], this function also is useful to solve the 2-loop RG equations (referred there to as ‘‘Laplace space’’).

2.4 Behavior at small momentum

While the theoretical expressions in the QCD factorization approach probe the logarithmic moments $L_n(\mu)$, typical applications of light-cone sum rules (LCSR) with B -meson LCDAs [4–7] require knowledge of the B -meson LCDAs for small momenta $\omega \leq s_0/2E$. Here s_0 is the effective threshold parameter in the hadronic model for the spectral density under consideration, and E is the large recoil energy of the physical process. In such applications we may expand the LCDA around $\omega = 0$, in terms of its n^{th} derivatives, assuming that the latter exist. We then obtain

$$\phi_+^{(n)}(0; \mu) = \frac{(-1)^{n+1}}{\Gamma(n)} \int_0^\infty ds s^n \eta_+(s; \mu) = -\frac{(-\hat{\mu}_m)^{-n}}{\Gamma(n)} F_{[\eta_+]}(-n; \mu) \quad (2.25)$$

with the same generating function $F_{[\eta_+]}(t)$. It is to be stressed here that $\phi_+^{(n)}(0)$ discussed above probe the function $F_{[\eta_+]}$ at finite (discrete) values $t = -n$ ($n > 0$), while the previously discussed logarithmic moments L_n probe the Taylor coefficients of the function $F_{[\eta_+]}$ around $t = 0$. Thus, LCSR and QCD factorization calculations are sensitive to different features of the underlying LCDA $\phi_+(\omega)$. In particular, for phenomenological applications beyond the leading factorizable terms, it is not sufficient to consider only the behavior at $t = 0$ without also considering the behavior at $t = -n$. On this point we disagree with the conclusions drawn in ref. [18] where it has been argued that only the expansion of the function $F_{[\phi_+]}(t)$ around $t = 0$ is phenomenologically relevant.

We finally note that in the context of LCSR it has been observed that the strict expansion of the sum rule in $s_0/2E \ll 1$ is numerically not well converging. In this view, we propose another quantity to benchmark parametrizations of the LCDA, the normalized Laplace transform⁵

$$\frac{\mathcal{L}[\phi_+](\zeta, \mu)}{\mathcal{L}[\omega](\zeta)} \equiv \frac{\int_0^\infty d\omega e^{-\zeta\omega} \phi_+(\omega, \mu)}{\int_0^\infty d\omega e^{-\zeta\omega} \omega} = \zeta^2 \tilde{\phi}_+(-i\zeta, \mu). \quad (2.26)$$

For $\zeta \rightarrow \infty$ this reduces to $\phi_+'(0)$, while for large but finite values of ζ one is sensitive to the low ω -behavior of the LCDA, regardless of whether the derivatives $\phi_+^{(n)}(0)$ exist.

3 Parametrization of the B -meson LCDA

We propose a novel parametrization of the leading-twist B -meson LCDA that fulfills the properties discussed in section 2. We start from the position-space LCDA and study the function $\chi[r]$ defined by the integral

$$\chi[r](\mu) \equiv \int_{-\infty}^\infty \frac{d\tau}{2\pi} \left| \tilde{\phi}_+(\tau; \mu) \right|^2 |r(\tau; \mu)|^2 \quad (3.1)$$

⁵This is not to be confused with what is referred to as the *Laplace transform* in ref. [18], which we call the *generating function*; see eq. (2.17).

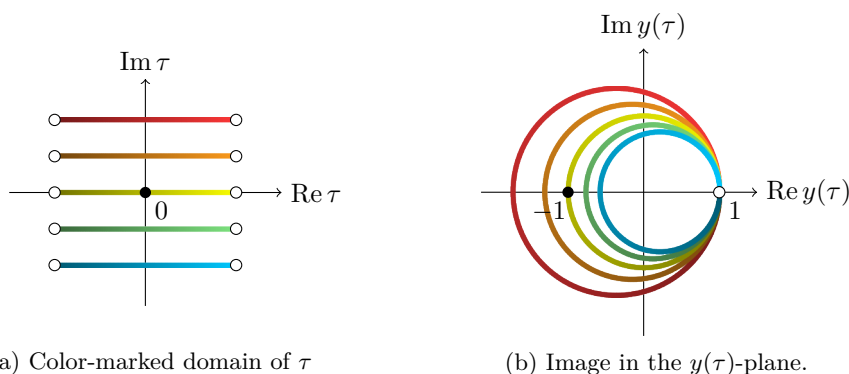


Figure 1. Illustration of the variable transform $\tau \mapsto y(\tau)$, with τ in units of $1/\omega_0$. Hollow small circles are understood to represent points at $\text{Re } \tau \rightarrow \pm\infty$. The small circles and colored lines correspond to each other in the left and right sketches.

with some suitably chosen complex function $r(\tau; \mu)$. It is instructive to rewrite this integral by means of the variable transform

$$\tau \mapsto y(\tau) \equiv \frac{i\omega_0\tau - 1}{i\omega_0\tau + 1} \quad \Leftrightarrow \quad i\omega_0\tau(y) = \frac{1+y}{1-y}. \quad (3.2)$$

This introduces an auxiliary parameter ω_0 , which serves as a reference momentum scale. The variable transform features the following properties, which are visualized in figure 1.

- The point $\tau = 0$ is mapped onto $y(\tau = 0) = -1$.
- The points at $|\tau| \rightarrow \infty$ are mapped onto $\lim_{|\tau| \rightarrow \infty} y(\tau) = +1$.
- The real τ axis is mapped onto the standard unit circle $|y| = 1$ in the complex y -plane.
- The half plane $\text{Im } \tau < 0$ is mapped onto the open unit disk $|y| < 1$.

Using the new variable y , the integral in eq. (3.1) is mapped onto the integral along the boundary ∂D of the unit disc in the complex y plane

$$\begin{aligned} \chi[r] &= \oint_{\partial D} \frac{dy}{2\pi} \left| \tilde{\phi}_+(\tau(y)) \right|^2 |r(\tau(y))|^2 J(\tau(y)) \\ &= \int_{-\pi}^{\pi} \frac{d\theta}{2\pi} \left| \tilde{\phi}_+(\tau(y)) \right|^2 |r(\tau(y))|^2 (-iy) J(\tau(y)) \Big|_{y=e^{i\theta}}. \end{aligned} \quad (3.3)$$

In the above $\theta = \arg(y)$ and we drop the scale dependence in the arguments for legibility. The Jacobian $-iyJ$ of the chain of variable transforms reads

$$-iy J(\tau(y)) = -iy \frac{d\tau}{dy} = -\frac{2y}{\omega_0(1-y)^2} = \frac{1 + \omega_0^2\tau^2}{2\omega_0}. \quad (3.4)$$

This result inspires us to factorize the LCDA as

$$\tilde{\phi}_+(\tau) \equiv \frac{f_+(y(\tau))}{r(\tau)(1+i\omega_0\tau)}, \quad \tilde{\phi}_+^*(\tau) = \frac{f_+^*(y^*(\tau))}{r^*(\tau)(1-i\omega_0\tau)}. \quad (3.5)$$

This factorization simplifies the expression in eq. (3.1)

$$\chi = \frac{1}{2\omega_0} \int_{-\pi}^{\pi} \frac{d\theta}{2\pi} |f_+(y)|^2 \Big|_{y=e^{i\theta}}, \quad (3.6)$$

which is similar in construction to unitarity bounds for hadronic form factors and is therefore conducive to a systematic parametrization of ϕ_+ (or equivalently f_+) in terms of orthogonal polynomials on the y unit circle; see ref. [24] and references therein. These polynomials coincide with the monomials y^n . Negative powers of y cannot appear in the parametrization of $\phi(\tau)$, since they would induce singularities on the open unit disk, thereby violating **P1**. The same holds for positive powers of y^* . Therefore, the Taylor expansion of the function $f_+(y)$ corresponds to the Fourier series

$$f_+(y) \equiv \sum_{k=0}^{\infty} a_k y^k, \quad f_+(y)|_{y=e^{i\theta}} = \sum_{k=0}^{\infty} a_k e^{i\theta k} \quad (3.7)$$

which yields

$$\chi[r] = \frac{1}{2\omega_0} \sum_{k=0}^{\infty} |a_k|^2. \quad (3.8)$$

Therefore the sequence $\{a_k\}$ is an element of the ℓ^2 space of sequences and must fall off faster than $\sqrt{1/k}$ as $k \rightarrow \infty$. In this way we have constructed a converging expansion for the LCDA in position space. The expansion can be truncated at some value $k = K$, and the truncation error is controlled by the value of the integral $2\omega_0\chi$. From a different point of view, as the partial series is monotonously growing with K , a higher saturation due to the truncated parameters implies a better approximation by the truncated parametrisation. In contrast to the unitarity bounds for hadronic form factors, however, the value of the bound $\chi[r]$ for the leading-twist LCDA is presently not known. We find that $\chi[r]$ is finite as long as⁶

- $|\lim_{\tau \rightarrow \infty} r(\tau; \mu)/\tau| < \infty$, by **P4**; and
- $r(\tau; \mu)$ is regular as $\tau \rightarrow 0$, by **P2**.

As our default choice for the weight function r we take the simplest form that is consistent with the analyticity requirements of $\tilde{\phi}_+(\tau)$ and that leads to at least a $1/\tau^2$ suppression of $\tilde{\phi}_+(\tau)$ for $|\tau| \rightarrow \infty$, see **P4**,

$$r(\tau; \mu_0) \equiv 1 + i\omega_0\tau, \quad (3.9)$$

at a *fixed* reference scale μ_0 for which we require that $\mu_0/\omega_0 \sim \mathcal{O}(1)$. Other choices for $r(\tau, \mu_0)$ can be reduced to eq. (3.9) by readjusting the parameters a_n in the truncated expansion in y . Note that the choice of the weight function is neither unique nor meaningful for the expansion of the LCDA to infinite order in our basis — it is critical, however,

⁶Indeed it is sufficient that $r(\tau; \mu)$ diverges slower than $1/\sqrt{\tau}$ for $\tau \rightarrow 0$, i.e. $\lim_{\tau \rightarrow 0} \sqrt{\tau} r(\tau) = 0$.

for the rate of convergence. We preemptively point out that our choice reproduces the popular exponential model at trivial order, i.e., $a_0 = 1$ and $a_{k>0} = 0$ for some value of ω_0 . Thus one can view our parametrisation as a systematic extension of the exponential model. Via eq. (2.9) our choice for $r(\tau, \mu_0)$ leads to simple expressions for the dual LCDA, see below. With this — as one of the central results of our paper — we obtain the following parametrization of the B -meson LCDA in position space,

$$\begin{aligned}\tilde{\phi}_+(\tau; \mu_0) &= \frac{(1 - y(\tau))^2}{4} \sum_{k=0}^K a_k(\mu_0) (y(\tau))^k \\ &= \frac{1}{(1 + i\omega_0\tau)^2} \sum_{k=0}^K a_k(\mu_0) \left(\frac{i\omega_0\tau - 1}{i\omega_0\tau + 1} \right)^k,\end{aligned}\tag{3.10}$$

which reflects an expansion in the point $\tau = -i/\omega_0$. It is to be emphasized that our parametrization does not aim to cover the singular behavior of the LCDA in the local limit $\tau \rightarrow 0$. Actually, as can be seen from eq. (3.10), the values of $\tilde{\phi}(\tau)$ and all of its derivatives are finite at $\tau = 0$ for any finite value of the truncation K , which in turn implies the existence of all non-negative moments $\langle \omega^n \rangle$ in momentum space. Nevertheless — as we will show in section 4 — the parametrization can be used at small but *finite* values $|\tau_0| \sim 1/\mu_0 \ll 1/\omega_0$ to implement the constraints from the local OPE on $\tilde{\phi}_+(\tau, \mu_0)$ [25]. In this way, we can also mimic the “radiative tail” for intermediate values $\omega \sim \mu_0 \gg \omega_0$ of the B -meson LCDA in momentum space [12]. Moreover, as we show below, we can consistently include the RG evolution within the framework of our parametrization by suitably adjusting the coefficients $a_k(\mu)$ and the function $r(\tau, \mu)$.

3.1 LCDA in dual space and logarithmic moments

In dual space our parametrization proposed in eq. (3.10) translates via eq. (2.9) to

$$\eta_+(s; \mu_0) = e^{-s\omega_0} \sum_{k=0}^K \frac{(-1)^k a_k(\mu_0)}{1+k} L_k^{(1)}(2\omega_0 s),\tag{3.11}$$

where $L_k^{(1)}$ are the associated Laguerre polynomials. The expansion coefficients can be obtained from the orthogonality of the Laguerre polynomials resulting in the projection

$$a_k(\mu_0) = 4(-1)^k \omega_0 \int_0^\infty ds (\omega_0 s) e^{-s\omega_0} L_k^{(1)}(2\omega_0 s) \eta_+(s; \mu_0).\tag{3.12}$$

The expression for the integral χ reads

$$\begin{aligned}2\omega_0 \chi[r](\mu_0) &= \sum_{k=0}^K |a_k|^2 = 2\omega_0 \int_0^\infty ds \left(\omega_0^2 |s\eta_+(s; \mu_0)|^2 + \left| \frac{d}{ds} (s\eta_+(s; \mu_0)) \right|^2 \right) \\ &\equiv 2\omega_0 \int_0^\infty ds \int_0^\infty ds' (s'\eta_+^*(s'; \mu_0)) R_{[\eta]}(s', s) (s\eta_+(s; \mu_0)),\end{aligned}\tag{3.13}$$

with the corresponding integral transform of our default choice of $|r(\tau; \mu_0)|^2$,

$$R_{[\eta]}(s', s) = \omega_0^2 \delta(s - s') - \delta''(s - s').\tag{3.14}$$

The generating function for the logarithmic moments can be expressed as

$$F_{[\eta_+]}(t; \mu_0, \mu_m) = \frac{\Gamma(1-t)}{\omega_0} \left(\frac{\hat{\mu}_m}{\omega_0} \right)^{-t} \sum_{k=0}^K a_k {}_2F_1(-k, 1+t; 2; 2). \quad (3.15)$$

This result can be obtained using Cauchy's residue theorem, where poles of higher order result in derivatives of the integrand, which can be expressed in terms of binomial coefficients. The hypergeometric function with negative first argument simplifies to polynomials in t of n^{th} order,

$${}_2F_1(0, 1+t; 2; 2) = 1, \quad {}_2F_1(-1, 1+t; 2; 2) = -t, \quad {}_2F_1(-2, 1+t; 2; 2) = \frac{1}{3}(1+2t^2), \quad \text{etc.}, \quad (3.16)$$

which are even functions of t for even n , and odd functions of t for odd n . From this we obtain the expressions for the first few logarithmic moments within our parametrization:

$$L_0(\mu_0) = \frac{1}{\omega_0} \sum_{k=0}^K \frac{1 - (-1)^{k+1}}{2} \frac{a_k(\mu_0)}{k+1} = \frac{a_0 + a_2/3 + \dots}{\omega_0}, \quad (3.17)$$

$$\begin{aligned} L_1(\mu_0) &= - \left(\ln \frac{\hat{\mu}_m}{\omega_0} - \gamma_E \right) L_0(\mu_0) + \frac{1}{\omega_0} \sum_{k=0}^K a_k \left[\frac{d}{dt} {}_2F_1(-k, 1+t; 2; 2) \right]_{t=0}, \quad (3.18) \\ &= - \left(\ln \frac{\hat{\mu}_m}{\omega_0} - \gamma_E \right) L_0(\mu_0) + \frac{-a_1 - 2/3 a_3 + \dots}{\omega_0}, \end{aligned}$$

$$\begin{aligned} L_2(\mu_0) &= \left[\frac{\pi^2}{6} - \left(\ln \frac{\hat{\mu}_m}{\omega_0} - \gamma_E \right)^2 \right] L_0(\mu_0) - 2 \left(\ln \frac{\hat{\mu}_m}{\omega_0} - \gamma_E \right) L_1(\mu_0) \quad (3.19) \\ &\quad + \frac{1}{\omega_0} \sum_{k=0}^K a_k \left[\frac{d^2}{dt^2} {}_2F_1(-k, 1+t; 2; 2) \right]_{t=0}, \\ &= \left[\frac{\pi^2}{6} - \left(\ln \frac{\hat{\mu}_m}{\omega_0} - \gamma_E \right)^2 \right] L_0(\mu_0) - 2 \left(\ln \frac{\hat{\mu}_m}{\omega_0} - \gamma_E \right) L_1(\mu_0) \\ &\quad + \frac{4/3 a_2 + 4/3 a_4 + 56/45 a_6 + \dots}{\omega_0}. \end{aligned}$$

We emphasize that the properties of the confluent hypergeometric functions appearing in eq. (3.18) and eq. (3.19) induce for $\mu_m = \omega_0 e^{-\gamma_E}$ that the logarithmic moments L_0 and L_2 only depend on coefficients a_k with even index k . Likewise, the logarithmic moment L_1 only depends on coefficients a_k with odd index k . The sequence generated by the hypergeometric functions and their derivatives is a null sequence. This brings along two important properties:

1. convergence of the series representation of the logarithmic moments is possible, even if the series $\sum_k a_k$ were not convergent; and
2. at the reference scale $\mu_m = \omega_0 e^{-\gamma_E}$, the logarithmic moments L_0 and L_1 can be chosen independently of each other, i.e., there is no model correlation between the two even for a truncated expansion.

3.2 Momentum-space LCDA and behavior at $\omega = 0$

The Fourier transform of our parametrisation in eq. (3.10) yields the corresponding expansion of the momentum-space LCDA in terms of generalized Laguerre polynomials:

$$\phi_+(\omega; \mu_0) = \frac{\omega e^{-\omega/\omega_0}}{\omega_0^2} \sum_{k=0}^K \frac{a_k(\mu_0)}{1+k} L_k^{(1)}(2\omega/\omega_0). \quad (3.20)$$

The expansion coefficients can be obtained from the orthogonality of the Laguerre polynomials resulting in the projection

$$a_k(\mu_0) = 4 \int_0^\infty d\omega e^{-\omega/\omega_0} L_k^{(1)}(2\omega/\omega_0) \phi_+(\omega; \mu_0). \quad (3.21)$$

Alternatively, they can be obtained as the series coefficients of a single integral expression,

$$a_k(\mu_0) = \frac{1}{k!} \frac{\partial^k}{\partial t^k} \int_0^\infty d\omega \frac{4}{(1-t)^2} \exp\left\{\frac{(t+1)\omega}{(t-1)\omega_0}\right\} \phi_+(\omega; \mu_0) \Big|_{t=0}. \quad (3.22)$$

We highlight that truncating the parametrization at $K = 0$ and fixing $a_0 = 1$ yields the popular exponential model [11]. We emphasize again that the auxiliary parameter ω_0 in our parametrization has no physical meaning and only serves as a reference scale, which does, however, influence the convergence of the expansion. The integral $\chi[r]$ can be expressed in terms of the momentum-space LCDA as

$$\begin{aligned} 2\omega_0 \chi[r](\mu_0) &= \sum_{k=0}^K |a_k|^2 = 2\omega_0 \int_0^\infty d\omega \left(|\phi_+(\omega; \mu_0)|^2 + \omega_0^2 \left| \frac{d\phi_+(\omega; \mu_0)}{d\omega} \right|^2 \right) \\ &\equiv 2\omega_0 \int_0^\infty d\omega \int_0^\infty d\omega' \phi_+^*(\omega'; \mu_0) R_{[\phi]}(\omega', \omega) \phi_+(\omega; \mu_0) \end{aligned} \quad (3.23)$$

with the Fourier transform of our default choice of $|r(\tau; \mu_0)|^2$,

$$R_{[\phi]}(\omega', \omega) = \delta(\omega - \omega') - \omega_0^2 \delta''(\omega - \omega'). \quad (3.24)$$

We note the similarity with the corresponding expressions in eq. (3.14), which strengthens the notion of $\eta_+(s)$ being a “dual space representation” of $\phi_+(\omega)$.

The Taylor expansion of $\phi_+(\omega; \mu_0)$ around $\omega = 0$ is related to our expansion coefficients as follows:

$$\begin{aligned} \phi_+'(0; \mu_0) &= \frac{1}{\omega_0^2} \sum_{k=0}^\infty a_k, \\ \phi_+''(0; \mu_0) &= -\frac{1}{\omega_0^3} \sum_{k=0}^\infty (2k+2) a_k, \quad \text{etc.} \end{aligned} \quad (3.25)$$

where the coefficients a_k in the expressions for the n^{th} derivative are weighted by numbers growing power-like with k^{n-1} . Since $\phi_+'(0)$ exists, the coefficients a_k must either have alternating signs, or they must fall off faster than $1/k$. However, we cannot constrain the convergence of the series representation for the higher derivatives in eq. (3.25).

As already mentioned above, one should keep in mind that actual applications of B -meson LCDA in QCD sum rules consider *integrals* of $\phi_+(\omega)$ over a finite interval of small ω values. Typically, the integrals are computed after Borel transformation, such that the appearing expressions are Laplace transformations of the momentum space representation $\phi_+(\omega)$. For this reason we consider the normalized Laplace transformation of $\phi_+(\omega)$ in eq. (2.26) at large values $\zeta \equiv n t_0$ as an example,

$$\ell_n(\mu, t_0) \equiv n^2 t_0^2 \tilde{\phi}_+(-int_0; \mu) \tag{3.26}$$

$$\ell_n(\mu, 1/\lambda_B) = \frac{1}{\lambda_B^2} \frac{n^2}{(1 + n\omega_0/\lambda_B)^2} \sum_{k=0}^{\infty} a_k(\mu) \left(\frac{n\omega_0/\lambda_B - 1}{n\omega_0/\lambda_B + 1} \right)^k \tag{3.27}$$

The expansion of the quantities ℓ_n in terms of the coefficients a_k in our parametrization converges for $0 < n < \infty$.

3.3 RG evolution

At one-loop accuracy, the RG evolution is multiplicative in dual space. Starting from our default parametrization at a fixed scale μ_0 we obtain

$$\eta_+(s; \mu) = e^{V(\mu, \mu_0)} (\hat{\mu}_0 s)^{-g(\mu, \mu_0)} e^{-s\omega_0} \sum_{k=0}^K \frac{(-1)^k a_k(\mu_0)}{1+k} L_k^{(1)}(2\omega_0 s). \tag{3.28}$$

We discuss three different ways of implementing the above scale evolution for our parametrisation:

1. Use the above equation as is, that is to say, the respective forms in momentum and position space. The expansion of $\phi_+(\omega, \mu)$ remains in terms of the coefficients $a_k(\mu_0)$ while the basis of functions of the parametrisation changes.
2. Project eq. (3.28) onto our parametrisation *with our default choice of $r(\tau)$* . We obtain a matrix

$$a_{k'}(\mu) \sim \sum_{k=0}^K \mathcal{R}_{k'k} a_k(\mu_0), \quad k' = 0, 1, \dots, \infty.$$

Put differently, the basis of functions remains the same at all scales while the coefficients evolve. In this approach, starting with a truncated set of coefficients $a_k(\mu_0)$, $k \leq K$, the evolution generates an *infinite set* of coefficients $a_{k'}(\mu)$. For practical applications, we thus need to truncate a second time ($k' \leq K'$). The requirements for the secondary truncation parameter K' can be studied numerically.

3. Project eq. (3.28) onto a modified parametrisation *with a scale-dependent choice of $r(\tau, \mu) = \tilde{r}$* . The function \tilde{r} is chosen such that we achieve a coefficient RGE similar to the previous approach, with the additional feature that $K' = K$ by construction, i.e., no secondary truncation is necessary:

$$\tilde{a}_{k'}(\mu) \sim \sum_{k=0}^K \tilde{\mathcal{R}}_{k'k} a_k(\mu_0), \quad k' = 0, 1, \dots, K,$$

with $\tilde{a}_k(\mu_0) = a_k(\mu_0)$. This approach guarantees that the coefficients remain bounded, $|\tilde{a}_k(\mu)| < \sqrt{2\omega_0 \tilde{\chi}(\mu)}$ at any scale μ , where $\tilde{\chi} \equiv \chi[\tilde{r}]$.

From now on we abbreviate $g \equiv g(\mu, \mu_0)$ and $V \equiv V(\mu, \mu_0)$.

First, transforming eq. (3.28) into momentum space, we obtain:

$$\phi_+(\omega; \mu) = e^V \left(\frac{\hat{\mu}_0}{\omega_0} \right)^{-g} \frac{\omega}{\omega_0^2} \sum_{k=0}^K (-1)^k \frac{a_k(\mu_0)}{1+k} \left[\frac{1}{k!} \frac{d^k}{dt^k} \left(\frac{1-t}{1+t} \right)^{-g} \frac{\Gamma(2-g)}{(1+t)^2} {}_1F_1 \left(2-g; 2; \frac{t-1}{t+1} \frac{\omega}{\omega_0} \right) \right]_{t=0}. \quad (3.29)$$

The derivatives produce an expansion in ${}_1F_1(n-g; n; -x)$, where ${}_1F_1(n-g; n; -x) \rightarrow e^{-x}$ for $g \rightarrow 0$. Here, the coefficients $a_k(\mu_0)$ fulfill a bound obtained at the initial scale. Numerical calculations using the LCDA require evaluations of the hypergeometric functions with non-integer parameters. Obviously, this procedure is not very convenient for numerical evaluation, especially when taking the necessary variation of ω_0 into account.

For the second case we obtain:

$$a_{k'}(\mu) = e^V \left(\frac{\hat{\mu}_0}{2\omega_0} \right)^{-g} \sum_{k=0}^K \mathcal{R}_{k'k}(\mu, \mu_0) a_k(\mu_0), \quad (3.30)$$

where the matrix $\mathcal{R}(\mu, \mu_0)$ reads

$$\mathcal{R}_{k'k}(\mu, \mu_0) = \frac{(-1)^{k'+k}}{1+k} \int_0^\infty dz z^{1-g} e^{-z} L_{k'}^{(1)}(z) L_k^{(1)}(z) \quad (3.31)$$

$$= \Gamma(2-g) \frac{(-1)^{k'+k}}{(1+k)!k'!} \frac{d^k}{du^k} \frac{d^{k'}}{dv^{k'}} \frac{1}{(1-uv)^2} \left(\frac{1-uv}{(u-1)(v-1)} \right)^g \Big|_{u,v=0}, \quad (3.32)$$

with $\mathcal{R}_{k'k}(\mu_0, \mu_0) = \delta_{k'k}$. This approach is promising for calculation-intensive numerical applications: for fixed $\mu \neq \mu_0$, the matrix needs to be calculated only once for any given secondary truncation K' ; the ω_0 -dependence is simply multiplicative; and observables can fully benefit from the simple and efficient representation. A closer inspection of eq. (3.31) shows that the off-diagonal elements of \mathcal{R} are suppressed by $O(g, 1/|k' - k|)$, and therefore the secondary truncation $K' < \infty$ is justified. We quantitatively confirm at hand of a model in section 4.2 that stable convergence can be achieved in a realistic scenario, even when $K' \approx K$.

In the third case, we consider the transformation of eq. (3.28) to position space, which yields a new parametrization:

$$\tilde{\phi}_+(\tau; \mu) = e^V \Gamma(1-g) \left(\frac{\omega_0}{\hat{\mu}_0} \right)^g \left(\frac{1-y}{2} \right)^2 \left(\frac{1+y}{2} \right)^{-g} \sum_{k'=0}^{K'=K} \tilde{a}_{k'}(\mu) y^{k'}. \quad (3.33)$$

We emphasize the truncation at $K' = K$. The new coefficients read

$$\tilde{a}_{k'}(\mu) = \sum_{k=k'}^K \tilde{\mathcal{R}}_{k'k}(\mu, \mu_0) a_k(\mu_0). \quad (3.34)$$

The transformation is given by an upper triangular matrix

$$\tilde{\mathcal{R}}_{k'k}(\mu, \mu_0) = \begin{cases} \frac{(-1)^{1+k} \Gamma(k+g-k')}{(1+k) \Gamma(g-1-k') \Gamma(1+k-k') \Gamma(1+k')} & k' \geq k \\ 0 & \text{otherwise} \end{cases}. \quad (3.35)$$

From the prefactor in eq. (3.33) we can read off the desired function \tilde{r} :

$$\tilde{r} \equiv e^{-V} \frac{(i\hat{\mu}_0\tau)^g (1 + i\omega_0\tau)^{1-g}}{\Gamma(1-g)}. \quad (3.36)$$

Using this function

$$\tilde{\chi} = \int_{-\infty}^{\infty} \frac{d\tau}{2\pi} \left| \tilde{\phi}_+(\tau; \mu) \right|^2 |\tilde{r}(\tau)|^2 = \frac{1}{2\omega_0} \sum_{k'=0}^{K'=K} |\tilde{a}_{k'}(\mu)|^2. \quad (3.37)$$

This modification comes at the expense that the functional basis, especially in momentum space, becomes more complicated as g enters the parametrisation non-trivially. We remark in closing that this third approach works for the one-loop RG evolution. However, we do not expect it to work in the two-loop case, where the RG equation in dual space becomes inhomogeneous [16]. Moreover, evolving from μ_0 to a smaller scale $\mu < \mu_0$, one obtains $g < 0$, and the integral bound thus only exists as long as $g(\mu, \mu_0)$ stays larger than $-1/2$, see footnote 6. On the other hand, g remains positive for $\mu > \mu_0$, and the parametrization with the weight function eq. (3.36) can be used as long as $g < 1$.

3.4 Application to higher twist

At higher twist, further LCDAs contribute to the calculation of exclusive processes. Given sufficient knowledge about their analytic properties, our approach can and should be applied to these as well. Here we discuss briefly the application to the second two-particle LCDA of the B -meson, which is denoted as $\tilde{\phi}_-(\tau)$. It is commonly split into two terms, $\tilde{\phi}_-(\tau) = \tilde{\phi}_-^{(\text{WW})} + \tilde{\phi}_-^{(\text{tw}3)}$. The first term refers to the so-called Wandzura-Wilczek limit and is related to the leading-twist LCDA $\tilde{\phi}_+(\tau)$. The second term $\tilde{\phi}_-^{(\text{tw}3)}$ is genuinely of twist-three origin and is related to the three-particle LCDA at twist three [22, 26]. Below, we only discuss the Wandzura-Wilczek term, and therefore drop the superscripts for simplicity. Its RG equations can be found in ref. [27], see also ref. [28].

In position space, the equation of motion connecting the Wandzura-Wilczek term with the leading-twist LCDA reads (see e.g. [29])

$$\tilde{\phi}_+(\tau) = \tau \frac{d}{d\tau} \tilde{\phi}_-(\tau) + \tilde{\phi}_-(\tau). \quad (3.38)$$

We can rewrite this equation in terms of the variable y , which yields:

$$\frac{\tilde{\phi}_+(\tau(y))}{(1-y)^2} = \frac{1}{2} \frac{d}{dy} \left[\frac{1+y}{1-y} \tilde{\phi}_-(\tau(y)) \right]. \quad (3.39)$$

The solution to this differential equation can be expressed in terms of $f_+(y)$:

$$\begin{aligned} \tilde{\phi}_-(\tau(y)) &= 2 \frac{1-y}{1+y} \int_{-1}^y dx \frac{\tilde{\phi}_+(\tau(x))}{(1-x)^2} = \frac{1}{2} \frac{1-y}{1+y} \int_{-1}^y dx f_+(x) \\ &\equiv \frac{1}{2} \frac{1-y}{1+y} [f_-(y) - f_-(-1)]. \end{aligned} \quad (3.40)$$

The integration constant and the lower boundary are fixed by requiring that the local limit $y \rightarrow -1$ coincides with the local limit of $\tilde{\phi}_+(\tau)$.

Our parametrisation for $\tilde{\phi}_+$ translates to the following expansion of f_- :

$$f_-(y) = \sum_{k=0}^K \frac{a_k}{1+k} y^{1+k} = \int_0^y dx f_+(x). \quad (3.41)$$

The asymptotic behaviour of $\tilde{\phi}_-(\tau)$ for $|\tau| \rightarrow \infty$ is $1/\tau$, as expected. The coefficients a_k enter with $1/(1+k)$ suppression, yielding a more convergent expansion than for the leading-twist LCDA. Hence, the truncation error for $\tilde{\phi}_-$ is under the same level of control as for $\tilde{\phi}_+$.

We obtain for the momentum space representation of the Wandzura-Wilczek term in our parametrization:

$$\begin{aligned} \phi_-(\omega; \mu_0) &= \int_\omega^\infty \frac{d\eta}{\eta} \phi_+(\eta; \mu_0), \\ &= \frac{1}{\omega_0} \sum_{k=0}^K \frac{a_k(\mu_0)}{1+k} \sum_{i=0}^k \frac{(-2)^i}{i!} \binom{k+1}{k-i} \Gamma(1+i, \omega/\omega_0) \\ &= \frac{e^{-\omega/\omega_0}}{\omega_0} \left\{ a_0 + \frac{a_2}{3} - \left(a_1 + \frac{2a_2}{3} \right) \frac{\omega}{\omega_0} + \frac{2a_2}{3} \frac{\omega^2}{\omega_0^2} + \dots \right\}, \end{aligned} \quad (3.42)$$

where we obtain our result through integration of the explicit representation of the Laguerre polynomials. Closed solutions can be obtained by Fourier transformation of the basis functions that appear in eq. (3.40), e.g.,

$$\frac{1-y}{1+y} \mapsto \frac{1}{2\omega_0}, \quad \frac{1-y}{1+y}y \mapsto \frac{1}{2\omega_0} \left[-1 + 4e^{-\omega/\omega_0} \right], \quad \text{etc.} \quad (3.43)$$

4 Application to existing models

For phenomenological applications, simple models of the B -meson LCDAs at a low reference scale μ_0 are commonly used. These models typically feature a small number of parameters. Here, we study four of these models in regard to how they can be captured by our parametrization. Our selection of models is chosen to showcase a wide variety of behavior. For ease of comparison, we discuss each model in terms of the dimensionless ratio

$$\xi \equiv \frac{\omega_0}{\lambda_B^{\text{model}}(\mu_0)} > 0, \quad (4.1)$$

where ω_0 is the auxiliary scale in our general parametrization, and $\lambda_B^{\text{model}}(\mu_0)$ the prediction for the inverse moment in the specific model. In each case, the coefficients a_k are matched onto the respective model by means of eq. (3.21).

For each of the considered models, we study the saturation of four of the relevant quantities as a function of the order of truncation K . The saturation of a quantity X is defined as

$$\text{Sat}[X]_K \equiv \frac{\sum_{k=0}^K X|_k}{\sum_{k=0}^\infty X|_k}, \quad (4.2)$$

where $X|_k$ is the contribution by the coefficient a_k in our parametrization. In the following we use these quantities:

- the result for the integral χ , which provides the bound for the expansion parameters a_k in our parametrization,

$$\chi|_k \equiv \frac{1}{2\omega_0} |a_k|^2 \tag{4.3}$$

- the derivative of the momentum-space LCDA at the origin,

$$\phi'_+(0)|_k \equiv \frac{1}{\omega_0^2} a_k \tag{4.4}$$

- the normalized Laplace transform at $\zeta = n/\lambda_B$,

$$\ell_n|_k \equiv \frac{1}{\lambda_B^2} \frac{n^2}{(1+n\xi)^2} \left(\frac{n\xi-1}{n\xi+1} \right)^k a_k; \tag{4.5}$$

- the inverse logarithmic moment,

$$L_0|_k = \lambda_B^{-1}|_k \equiv \frac{1}{2\omega_0} \frac{1+(-1)^k}{1+k} a_k, \tag{4.6}$$

- and the normalized first logarithmic moment,

$$\sigma_B|_k \equiv -\lambda_B L_1(\mu_m = e^{-\gamma_E} \lambda_B)|_k = \begin{cases} -\ln \xi & k=0 \\ -\frac{a_k}{\xi} \left[\frac{d}{dt} {}_2F_1(-k, 1+t; 2; 2) \right]_{t=0} & k \geq 1 \text{ and odd} \\ 0 & k \geq 1 \text{ and even} \end{cases} \tag{4.7}$$

All of the above quantities, including the expansion coefficients a_k , are implicitly understood to be evaluated at a renormalisation scale $\mu = \mu_0$.

We further consider the “relative growth” of some of the quantities. It is defined as

$$\text{Gr}[X]_K \equiv \frac{X|_K}{\sum_{k=0}^K X|_k}. \tag{4.8}$$

For each model, we consider the relative growth of the contribution to the bound χ . We also apply the relative growth to any of the benchmark quantities defined above if said quantity is ill-defined for a specific model. The relative growth is also instrumental for model-independent phenomenological studies as a proxy for the corresponding saturation. Its reliability, however, can only be tested in model studies, as the convergence rate of the parametrisation is not known a priori.

4.1 Exponential model

A popular model that is commonly taken as a starting point for a phenomenological analysis is [11]

$$\phi_+(\omega, \mu_0) = \frac{\omega}{\lambda_B^2} e^{-\omega/\lambda_B} \quad [\text{exp. model}]. \quad (4.9)$$

Projecting onto our ansatz via eq. (3.21) yields the following result for the expansion coefficients:

$$a_k = (k+1) \left(\frac{2\xi}{1+\xi} \right)^2 \left(\frac{\xi-1}{\xi+1} \right)^k \quad [\text{exp. model}]. \quad (4.10)$$

They fall off exponentially for $\xi \neq 1$. For $\xi = 1$, the exponential model trivially matches onto our parametrization with $a_0 = 1$ and $a_{k>0} = 0$. The result for the first few coefficients as a function of ξ is plotted in figure 2a. We observe a rapid fall off of the magnitude of the coefficients a_k for $k > 2$ in the entire “benchmark interval”

$$1/2 \lesssim \xi \lesssim 2 \quad [\text{benchmark interval}] \quad (4.11)$$

This allows us to use the above interval to define an estimator for the inherent uncertainty of our parametrization, also for other models to be discussed in the following. The uncertainty estimate is illustrated in figure 2b, where we plot the resulting variation of the shape of the momentum-space LCDA for different levels of truncation. Again, already with $K = 2$ we find a very narrow envelope for the parametrized function.

The integral bound for the exponential model can be calculated explicitly, yielding a monotonous function of ξ ,

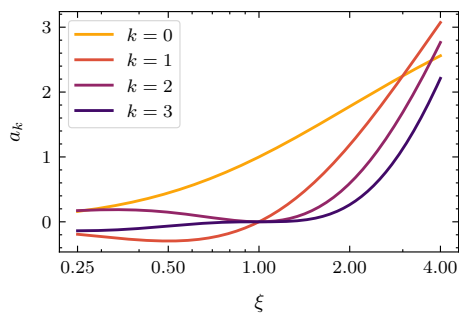
$$2\omega_0\chi = \frac{1}{2} (\xi + \xi^3) \quad [\text{exp. model}]. \quad (4.12)$$

We plot its saturation and its relative growth as a function of ξ in figure 2c and figure 2d, respectively, for different values of the truncation K . We observe that both the saturation and the relative growth give comparable information about the convergence of the parametrization. As expected, the convergence is very rapid as long as $\xi \simeq 1$: taking $K = 2$ and varying in the benchmark interval eq. (4.11), the saturation exceeds 98% and the relative growth is smaller than 7%.

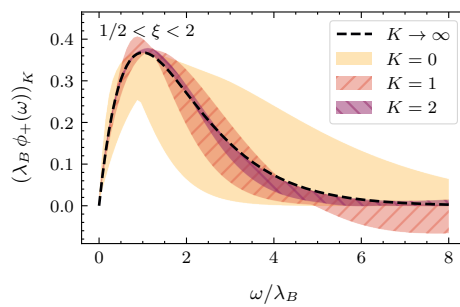
We continue to investigate the saturation for the inverse moment $L_0 = \lambda_B^{-1}$, which is plotted in figure 2e. This quantity also rapidly converges within our parametrization: for $K = 2$ the saturation within the benchmark interval is better than 98%. It is also instructive to study the normalized first logarithmic moment, which in the model is given by zero at the given scale μ_m ,

$$\sigma_B = 0 \quad [\text{exp. model}]. \quad (4.13)$$

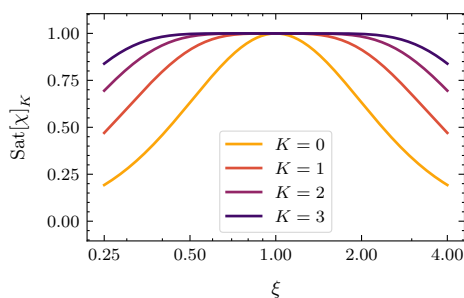
We show the result as a function of ξ for different truncations K in figure 2f. The model result is rapidly reproduced by the truncated parametrization, and the absolute difference falls below 0.11 for $K = 2$ in the benchmark interval.



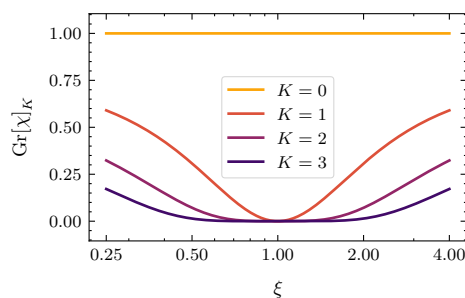
(a) Values for the expansion coefficients a_k



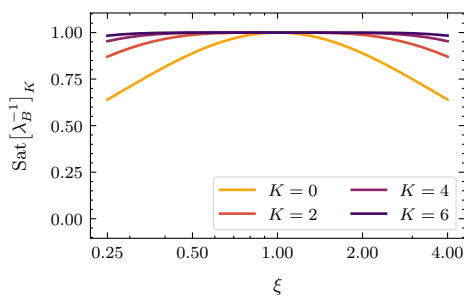
(b) Variability of the momentum-space LCDA for different truncations K in the interval $1/2 < \xi < 2$.



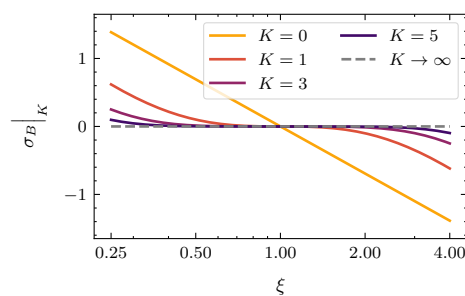
(c) Saturation of the integral bound χ



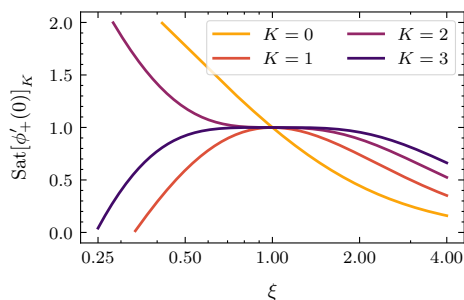
(d) Relative growth of the integral bound χ



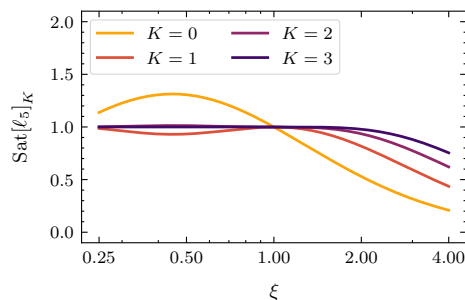
(e) Saturation of the inverse moment $L_0 = \lambda_B^{-1}$.



(f) Value of σ_B for different truncations K .



(g) Saturation of the derivative of $\phi_+(\omega)$ at the origin.



(h) Saturation of the normalized Laplace transform ℓ_5

Figure 2. Plots illustrating the truncation effects of our parametrization for the exponential model eq. (4.9). We often use the ratio $\xi = \omega_0/\lambda_B$, plotted on a logarithmic scale.

Finally, we study the saturation of the derivative of the LCDA at the origin $\omega = 0$ and of the normalized Laplace transform at $n = \zeta\lambda_B$. These test how well our parametrization captures the behavior of the LCDA at small light-cone momentum. In the exponential model, they read:

$$\phi'_+(0, \mu_0) = \lim_{n \rightarrow \infty} \ell_n = \frac{1}{\lambda_B^2}, \quad \ell_n(\mu_0, 1/\lambda_B) = \frac{1}{\lambda_B^2} \frac{n^2}{(1+n)^2} \quad [\text{exp. model}]. \quad (4.14)$$

In figure 2g and figure 2h we show the saturation of $\phi'_+(0)$ and ℓ_5 , respectively, for a number of different truncations K . We find for $K = 2$ in the benchmark interval $0.88 < \text{Sat}[\phi'_+(0)]_K < 1.19$ and $0.93 < \text{Sat}[\ell_5]_K < 1.02$. Because of the exponential decrease of the individual coefficients a_k in eq. (4.10), even $\phi'_+(0)$ shows a reasonable convergence. As discussed in section 3.2, the convergence of ℓ_5 is expected to be more rapid than for $\phi_+(0)$, which is confirmed by the plot.

We conclude that our parametrisation captures the exponential model with high precision even for small K . We remark that the parametrisation *to any order* envelopes the model *by construction*; however, the dependence on the auxiliary parameter ω_0 becomes weaker for growing K . We find that $K = 2$ offers sufficient precision for practical applications using the model.

Of course, an exemplary behavior of the relatively simple exponential model is expected, since it can be expressed to trivial order in K for the specific choice of $\omega_0 = \lambda_B$. Nevertheless, our analysis provides important input for the comparison with other models in the literature. For that comparison, the exponential model provides a benchmark.

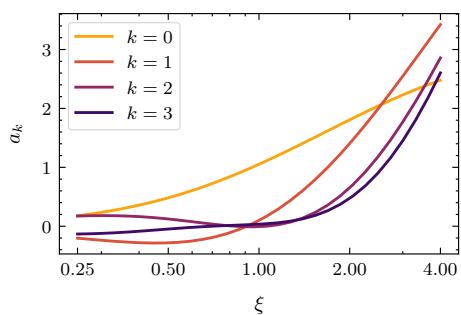
4.2 Lee-Neubert model with radiative tail

Lee and Neubert [12] have refined the exponential model by attaching a “radiative tail”, which can be deduced from the behavior of the partonic LCDA at large light-cone momenta $\omega \sim \mu \gg \Lambda_{\text{QCD}}$. In this model, the LCDA is described by an exponential at low values of ω , while a radiative tail is added at some intermediate value ω_t ,

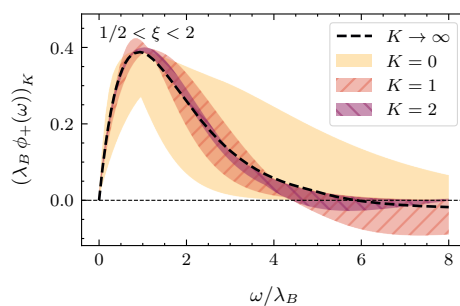
$$\phi_+(\omega, \mu) = \mathcal{N} \frac{\omega e^{-\omega/\bar{\omega}}}{\bar{\omega}^2} + \frac{\alpha_s C_F}{\pi} \frac{\theta(\omega - \omega_t)}{\omega} \left\{ \frac{1}{2} - \ln \frac{\omega}{\mu} + 4 \frac{\bar{\Lambda}_{\text{DA}}}{3\omega} \left(2 - \ln \frac{\omega}{\mu} \right) \right\} \quad [\text{Lee/Neubert}]. \quad (4.15)$$

Here $\bar{\Lambda}_{\text{DA}}$ is the HQET mass parameter in a convenient renormalon-free scheme, see ref. [12] for details. The parameter ω_t is fixed by requiring the model LCDA to be continuous at $\omega = \omega_t$, while the values for \mathcal{N} and $\bar{\omega}$ are fixed by matching to the partonic calculation. We stress that this model is not supposed to give the correct description at asymptotically large values $\omega \gg \mu$, which would require to further resum the large logarithms $\ln \omega/\mu$ in the above formula (see e.g. the discussion in ref. [23]). With this in mind, we match our parametrization to this model, and we aim at a reasonable description for small and intermediate values of ω . For the following numerical discussion, we adapt the parameter values found in ref. [12] for $\mu_0 = 1 \text{ GeV}$,

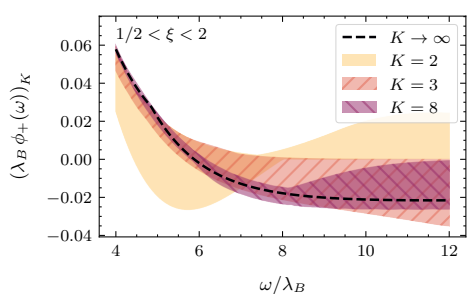
$$\bar{\Lambda}_{\text{DA}} = 519 \text{ MeV}, \quad \bar{\omega} = 438 \text{ MeV}, \quad \mathcal{N} = 0.963, \quad \omega_t = 2.33 \text{ GeV},$$



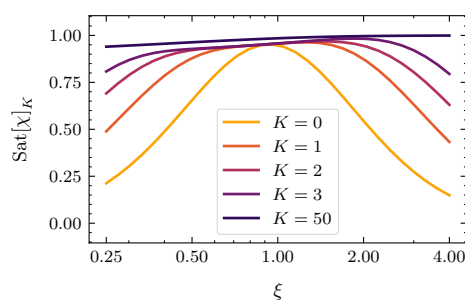
(a) Values for the expansion coefficients a_k .



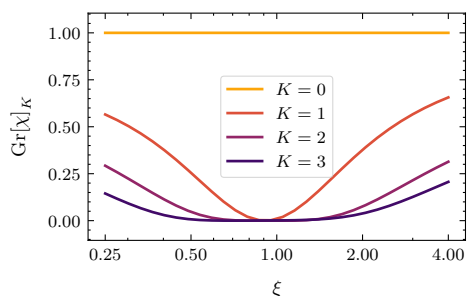
(b) Variability of the momentum-space LCDA for different truncations K in the interval $1/2 < \xi < 2$.



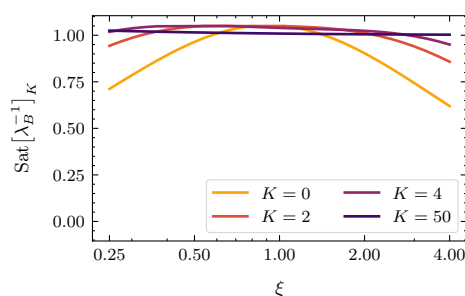
(c) Extension of 3b.



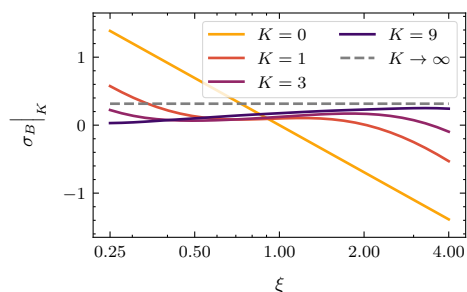
(d) Saturation of the integral bound χ .



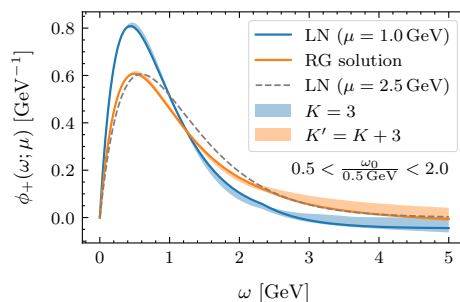
(e) Relative growth of the integral bound χ .



(f) Saturation of the inverse moment $L_0 = \lambda_B^{-1}$.



(g) Value of σ_B for different truncations K .



(h) Demonstration of the RG evolution.

Figure 3. Plots illustrating the truncation effects of our parametrization for the Lee-Neubert model eq. (4.15). We use the ratio $\xi = \omega_0/\lambda_B$, plotted on a logarithmic scale.

with $\alpha_s(\mu_0) = 0.5$. For this choice one finds

$$L_0 = \lambda_B^{-1} = 1/479 \text{ MeV}^{-1}, \quad \sigma_B = 0.315 \quad [\text{Lee/Neubert}], \quad (4.16)$$

and the expansion coefficients a_k can easily be calculated numerically. For instance, for $\xi = 1$ we find

$$a_0 \simeq 1.050, \quad a_1 \simeq 0.096, \quad a_2 \simeq -0.007, \quad a_3 \simeq 0.035, \quad a_4 \simeq -0.051, \quad a_5 \simeq 0.047.$$

For large values of k the coefficients a_k remain almost constant in magnitude, however, with alternating signs. The result for a_0, \dots, a_5 and the corresponding approximation to the Lee/Neubert model are shown in figure 3a and figure 3b, respectively. At first glance, the results look qualitatively very similar to the exponential model. However, the features induced by the radiative tail, namely the cusp at $\omega = \omega_t$ and the zero at $\omega \simeq 2.82 \text{ GeV}$, require special attention. We therefore zoom into the region $4 < \omega/\lambda_B < 12$ in figure 3c, where we also consider larger values for the truncation parameter K . We find that a reasonably precise description of the radiative tail at intermediate values of ω requires somewhat higher truncation levels than the exponential model. Note that — by construction — our parametrization is not designed to capture the radiative tail at values $\omega \gg \mu$. We will revisit this point later in section 5.

We continue with the discussion of the integral bound, which in the Lee-Neubert model takes the numerical value

$$2\omega_0\chi = 0.547\xi + 0.608\xi^3 \quad [\text{Lee/Neubert}], \quad (4.17)$$

which is close to the exponential model. We emphasize that the bound is finite due to the continuity of the model, despite the derivative in eq. (3.23) acting on the Heaviside distribution. The saturation and the relative growth of the integral bound are plotted in figure 3d and figure 3e, respectively. First, we observe that the saturation is always smaller than one; this is clear, as the bound is monotonously increasing with K . Second, we observe that the curves are tilted in comparison to the exponential model: small values of ξ result in slow convergence, while best convergence for the integral bound is obtained for values $\gtrsim 1$. The peaking structure reflects the fact that we need to include terms of higher order in k to get a reasonable description, such that the curve flattens. The relative growth of the bound plotted in figure 3e decreases reasonably within our benchmark interval $1/2 < \xi < 2$.

In figure 3f and figure 3g, we show the saturation for the inverse moment $L_0 = \lambda_B^{-1}$ and the value of σ_B as a function of ξ for different levels of truncation, respectively. Compared to the exponential model, we still find reasonable convergence for both quantities, however with a significantly lower rate and a clear preference for larger values of ξ .

We skip a discussion for $\phi'_+(0)$ and ℓ_5 , which show qualitatively the same behavior as in the exponential model. This is obvious, since they are naturally only sensitive to the region of small ω , where the radiative tail has no effect.

Next, we use the opportunity to demonstrate the RG evolution of the parameters as defined in eq. (3.30). Ref. [12] provides the model parameters for two different choices of the renormalisation scale and plots of the momentum-space LCDA, as well as the general

RG solution in momentum space. In figure 3h, we show the model at $\mu = 1$ GeV and its RG evolution to $\mu = 2.5$ GeV. They coincide well with our truncated parametrization with $K = 3$ at the initial scale and its evolution to $\mu = 2.5$ GeV with $K' = K + 3$, using the usual benchmark interval for $\xi = \omega/\lambda_B$ for illustration. We also plot the model as provided at $\mu = 2.5$ GeV purely for reference. Our plot is visually indistinguishable from the plots shown in ref. [12]. We further observe that the variation band is consistent for both scales, which verifies the expectation that higher orders in the expansion remain negligible.

4.3 Naïve parton model

In the naïve parton model [26] the LCDA takes the form

$$\phi_+(\omega) = \frac{\omega}{2\lambda_B^2} \theta(2\lambda_B - \omega) \quad [\text{parton model}], \quad (4.18)$$

where λ_B is identified with the HQET mass parameter $\bar{\Lambda} \simeq M_B - m_b$. In position space this yields

$$\tilde{\phi}_+(\tau) = \frac{(1 + 2i\lambda_B\tau) e^{-2i\lambda_B\tau} - 1}{2\lambda_B^2\tau^2} \quad [\text{parton model}], \quad (4.19)$$

which only falls off as $1/\tau$ for $|\tau| \rightarrow \infty$, thereby violating **P4**. The parton-model LCDA is therefore a pathological example of a model. Nevertheless, it can serve as a toy model to study under which circumstances our parametrization can also capture extreme examples.

To this end, we show the numerical result for the expansion coefficients and the resulting shapes of the momentum-space LCDA for different levels of truncation in figure 4a and figure 4b, respectively. Indeed, we observe that the expansion coefficients remain sizable even for large values of k , without any preferred value for the ratio ξ . This indicates a bad convergence of the expansion. Similarly, our estimate for the truncation uncertainty in figure 4b, reflected by the variation of ξ in the benchmark interval, is larger than in the exponential model. As expected, the triangular shape cannot be reproduced well, even for very high levels of truncation.

As $\tilde{\phi}(\tau)$ only falls off as $1/\tau$, the integral bound χ in eq. (3.1) does not exist for our choice of the function $r(\tau, \mu_0)$. In figure 4c we therefore only plot the diverging sum

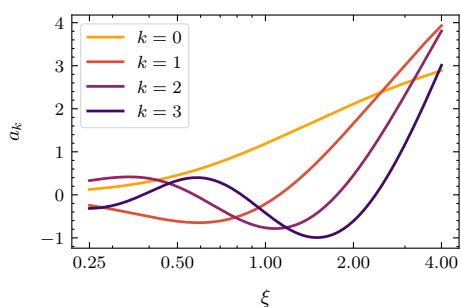
$$2\omega_0\chi|_K = \sum_{k=0}^K |a_k|^2,$$

together with its relative growth in figure 4d. The observed oscillatory behavior of the latter can be taken as an indicator for the non-convergence of the expansion.

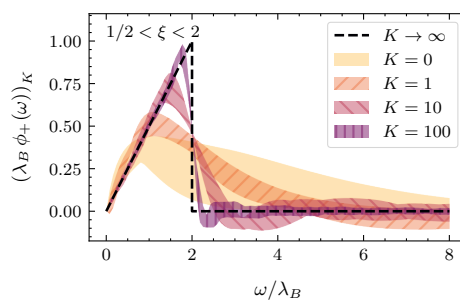
We continue with the discussion of $L_0 = \lambda_B^{-1}$ for which we plot the saturation in figure 4e. Its saturation oscillates around unity with an amplitude that is only slowly decreasing with increasing K . The normalized first logarithmic moment is given by

$$\sigma_B = 1 - \ln 2 - \gamma_E \simeq -0.270 \quad [\text{parton model}]. \quad (4.20)$$

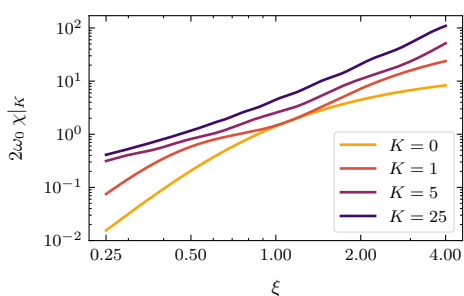
In figure 4f we show the result for different truncation K . Again we observe an oscillatory behavior around the true model value.



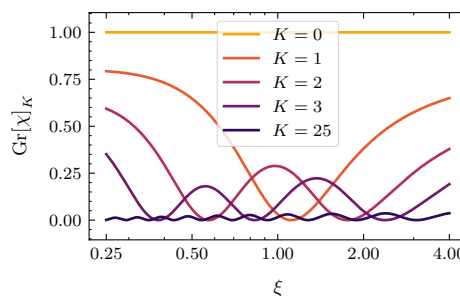
(a) Values for the expansion coefficients a_k .



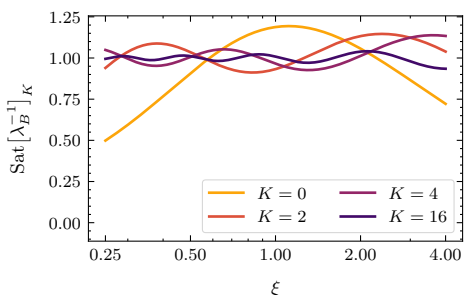
(b) Variability of the momentum-space LCDA for different truncations K in the interval $1/2 < \xi < 2$.



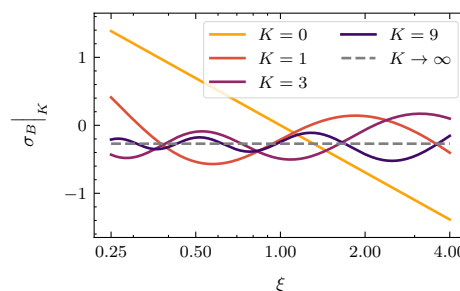
(c) Saturation of the integral bound χ .



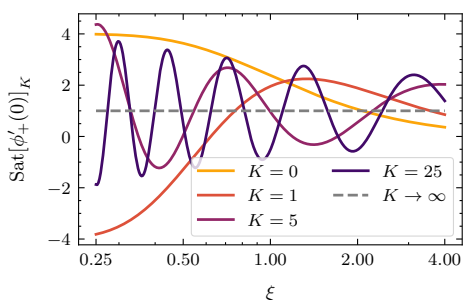
(d) Relative growth of the integral bound χ .



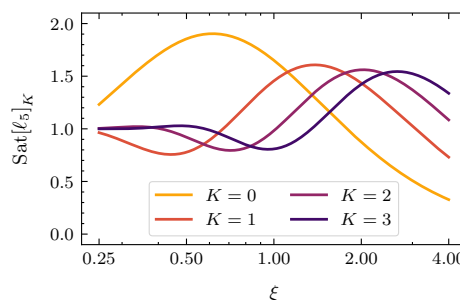
(e) Saturation of the inverse moment $L_0 = \lambda_B^{-1}$.



(f) Value of σ_B for different truncations K .



(g) Saturation of the derivative of $\phi_+(\omega)$ at the origin.



(h) Saturation of the normalized Laplace transform l_5 .

Figure 4. Plots illustrating the truncation effects of our parametrization for the parton model eq. (4.18). We often use the ratio $\xi = \omega_0/\lambda_B$, plotted on a logarithmic scale.

Finally, we study the convergence of our parametrization at low values of ω . We obtain

$$\phi'_+(0, \mu_0) = \frac{1}{2\lambda_B^2}, \quad \ell_n(\mu_0, 1/\lambda_B) = \frac{1}{2\lambda_B^2} \left(1 - (1 + 2n)e^{-2n}\right) \quad [\text{parton model}]. \quad (4.21)$$

The saturation of the derivative at the origin in figure 4g shows oscillatory behavior for the whole range of ξ , while for the normalized Laplace transform we observe that the saturation in figure 4h approaches unity for sufficiently large values of K and/or small values of ξ .

4.4 A model with $\phi'_+(\mathbf{0}) \rightarrow \infty$

Beneke et al. [10] have suggested to consider more general parametrizations for the B -meson LCDA, which also include cases where the derivative at the origin $\phi'_+(0)$ does not exist. We study their model

$$\phi_+(\omega, \mu_0) = \frac{1}{\Gamma(1+a)} \left(\frac{(1+a)\omega}{\lambda_B}\right)^{1+a} \frac{e^{-(1+a)\omega/\lambda_B}}{\lambda_B} \quad [\text{Beneke et al.}]. \quad (4.22)$$

For $a \rightarrow 0$, this function reduces to the simple exponential model. For $a < 0$, the behavior at $\omega \rightarrow 0$ is somewhat pathological, since it violates **P4**. Nevertheless, it is interesting to study the convergence of our parametrization for this behavior. For concreteness, in the following we only consider the case $a = -0.4$.

We show the coefficients a_k and the resulting shapes to the LCDA for different levels of truncation in figure 5a and figure 5b, respectively. We see that except for the vicinity of $\omega = 0$, already $K = 2$ yields a reasonable approximation within the estimated uncertainty from the ξ -variation.

The integral bound for the model follows as

$$2\omega_0\chi = \frac{1}{2^{1+2a}} \frac{\Gamma(2+2a)}{\Gamma(1+a)^2} \left(\xi + \frac{(1+a)^2}{1+2a} \xi^3\right)^{a \rightarrow -0.4} \simeq 0.360\xi + 0.649\xi^3 \quad [\text{Beneke et al.}]. \quad (4.23)$$

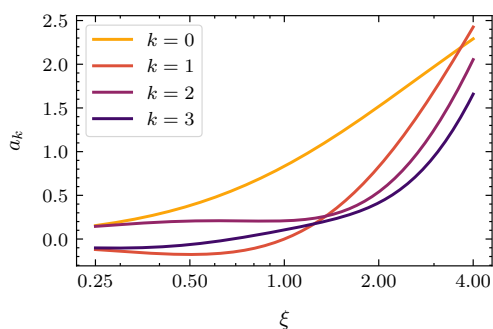
In figure 5c we observe the opposite behavior as compared to the Lee-Neubert model, i.e. the peak of the saturation is tilted to the other side, such that the best convergence is obtained for small values of ξ . Again, the relative growth of the integral bound in figure 5d remains small in the benchmark interval around $\xi = 1$.

The saturation of the inverse moment $L_0 = \lambda_B^{-1}$ and the normalized first logarithmic moment,

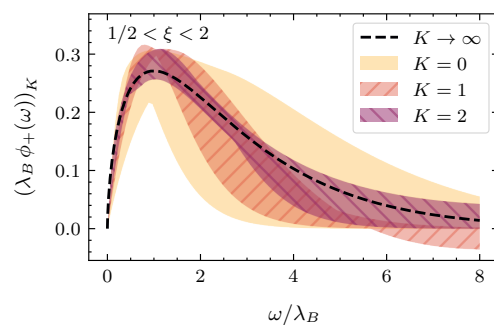
$$\sigma_B = -\Psi(1+a) + \ln(1+a) - \gamma_E \stackrel{a \rightarrow -0.4}{\simeq} +0.453 \quad [\text{Beneke et al.}], \quad (4.24)$$

are shown in figure 5e and figure 5f, respectively. Compared to the exponential model shown in figure 2e, the saturation for L_0 converges more slowly, and the truncated result for σ_B is rather sensitive to the value of ξ (for moderate truncation K).

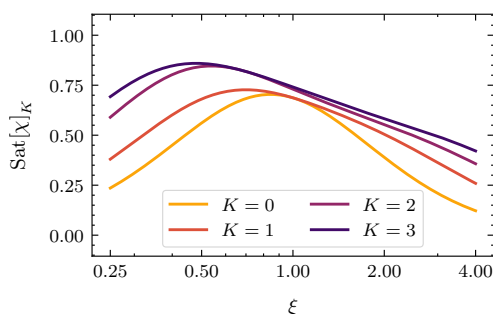
The fact that σ_B can be adjusted by an independent parameter a may be viewed as an advantage of the model eq. (4.22). However the required pathological behavior at



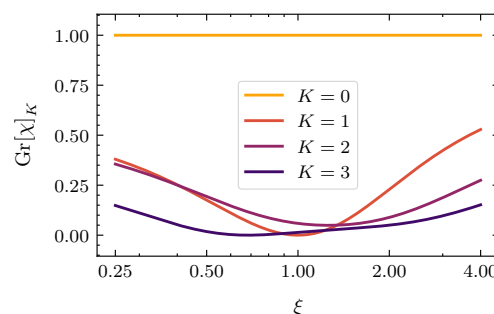
(a) Values for the expansion coefficients a_k .



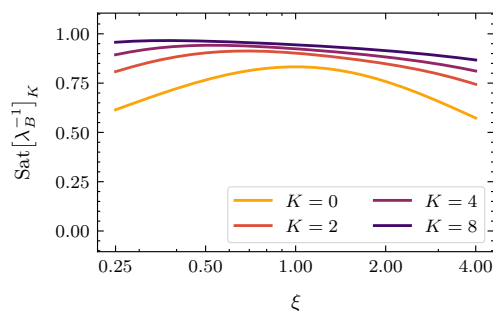
(b) Variability of the momentum-space LCDA for different truncations K in the interval $1/2 < \xi < 2$.



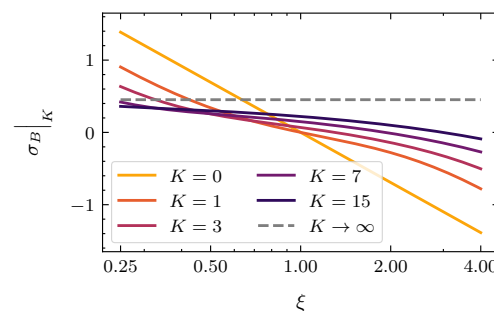
(c) Saturation of the integral bound χ .



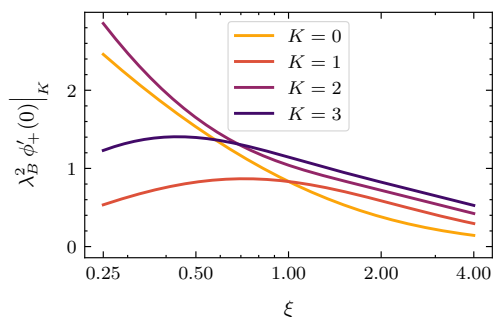
(d) Relative growth of the integral bound χ .



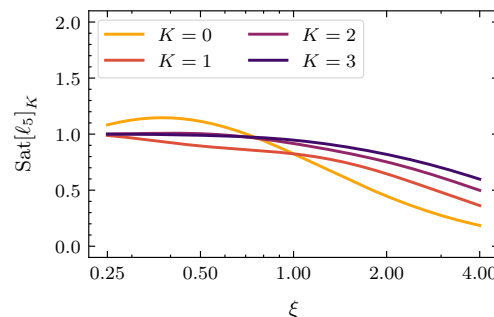
(e) Saturation of the inverse moment $L_0 = \lambda_B^{-1}$.



(f) Value of σ_B for different truncations K .



(g) Partial sum of the derivative at the origin.



(h) Saturation of the normalized Laplace transform ℓ_5 .

Figure 5. Plots illustrating the truncation effects of our parametrization for the model eq. (4.22) discussed by Beneke et al. [10]. We often use the ratio $\xi = \omega_0/\lambda_B$, plotted on a logarithmic scale.

$\omega \rightarrow 0$ makes it less useful in phenomenological applications. We therefore advocate our parametrization, which is able to systematically decorrelate the pseudo observables by including sufficiently many terms. We illustrate this point in the following section.

Finally, we also show the results for the quantities that characterize the behavior of the LCDA at small values of ξ . As the derivative at the origin does not exist in the model (4.22), in figure 5g we only show the truncated sum for a finite value of K ,

$$\phi'_+(0)_K = \frac{1}{\omega_0^2} \sum_{k=0}^K a_k.$$

Indeed, no convergence is apparent. In figure 5h, we show the saturation of the normalized Laplace transform,

$$\ell_n(\mu_0, 1/\lambda_B) = \frac{n^2}{\lambda_B^2} \left(\frac{1+a}{n+1+a} \right)^{2+a} \quad [\text{Beneke et al.}], \quad (4.25)$$

at $n = 5$. Here, we observe similarly good saturation properties as for the exponential model.

5 Pseudo-phenomenology

In this section we illustrate the feasibility of using our parametrization to describe the LCDA in its full kinematic range, based on a global analysis of all available phenomenological information in the future. Here, we do not strive for a rigorous statistical analysis. Instead, we illustrate the complementarity of the available constraints in a qualitative manner. Quantitative statements herein should not be mistaken for theoretical predictions.

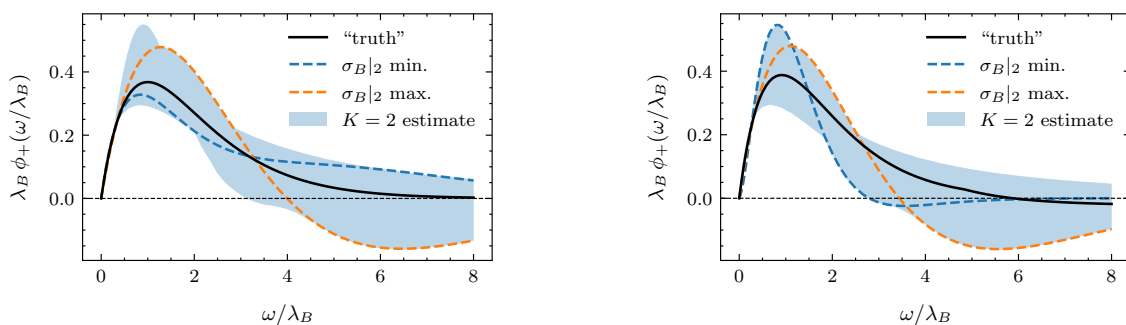
5.1 Using λ_B and ℓ_5 as phenomenological constraints

In this subsection we study the hypothetical situation that some phenomenological information, be it experimental or theoretical in nature, constrains the quantities (“pseudo observables”)

$$p_1 \equiv L_0(\mu_0, \mu_m) \quad \text{and} \quad p_2 \equiv \lambda_B^2 \ell_5(\mu_0, 1/\lambda_B) \quad (5.1)$$

at a low reference scale μ_0 . We select these two pseudo observables, because they emerge in the theoretical description of the $\bar{B}^- \rightarrow \gamma \mu^- \bar{\nu}$ form factors. An experimental determination of these form factors, through measurements of the decays, is foreseen by the Belle II experiment [3, 30, 31]. Moreover, these two pseudo observables probe complementary aspects of the B -meson LCDA: in the following discussion we will neglect the uncertainties on these parameters for simplicity. Of course, in a realistic fit to experimental data, these uncertainties as well as their correlations have to be taken into account. With no further theory input at hand, we can use our parametrization to estimate the effect on the B -meson LCDA and other derived quantities.

Here, we truncate at $K = 2$, which yields four independent parameters. They are ω_0 and a_0 through a_2 . With the two phenomenological constraints above, we can determine



(a) Using the exponential model eq. (4.9).

(b) Using the Lee-Neubert model eq. (4.15).

Figure 6. Pseudo-fit to the B -meson LCDA in momentum space using the two pseudo-observables $p_{1,2}$ as predicted by two models as a function of $x = \omega/\lambda_B$. We show the model (“truth”), the curves that lead to extreme values of σ_B and the total variation of the parametrized LCDA. For the latter, we take the benchmark interval for $\xi = \omega_0/\lambda_B$ and a small a_2 into account.

two of these parameters. We choose to determine a_0 and a_1 :

$$a_0 = \xi - \frac{a_2}{3}, \quad a_1 = \frac{(5\xi + 1)^3}{25(5\xi - 1)} p_2 - \frac{\xi(5\xi + 1)}{5\xi - 1} - \frac{2(25\xi^2 - 20\xi + 1)}{3(5\xi + 1)(5\xi - 1)} a_2,$$

where $\xi = p_1 \omega_0$.

(5.2)

This leaves two unconstrained parameters: the auxiliary scale ratio ξ and the coefficient a_2 . In order to constrain the possible ranges for ξ and a_2 , we now impose the following conditions, which are motivated by the findings in the previous subsection: the relative growth of the integral bound χ is limited to 20% (for $K = 1$) and 10% (for $K = 2$),

$$\frac{|a_1|^2}{|a_0|^2 + |a_1|^2} \leq 0.2, \quad \frac{|a_2|^2}{|a_0|^2 + |a_1|^2 + |a_2|^2} \leq 0.1.$$
(5.3)

Combined with eq. (5.2) this provides a bounded region for the joint distribution of the parameters ξ and a_2 . For any given pseudo observable we can therefore determine its minimal and maximal values for parameter values in that region.

For example, the result for the normalized logarithmic moment at the reference scale $\mu_m = 1/p_1 e^{-\gamma_E}$ is given by

$$\sigma_B|_2 \equiv -\frac{1}{p_1} L_1(\mu_0, 1/p_1 e^{-\gamma_E}) \Big|_{K=2} = -\ln \xi + \frac{a_1}{\xi}.$$
(5.4)

In the following, we will determine the resulting variations for the normalized logarithmic moment σ_B at $K = 2$, as well as for the LCDA $\phi(\omega)$ at different values of $x = \omega p_1$, and the normalized Laplace transformation ℓ_n at different (real) values of n for each of the four models discussed in section 4. Note that at this stage, the only difference between the four models is given by their predictions for the pseudo-observable p_2 , while the pseudo-observable p_1 only enters via the auxiliary parameter ξ to set the reference scale in the analysis.

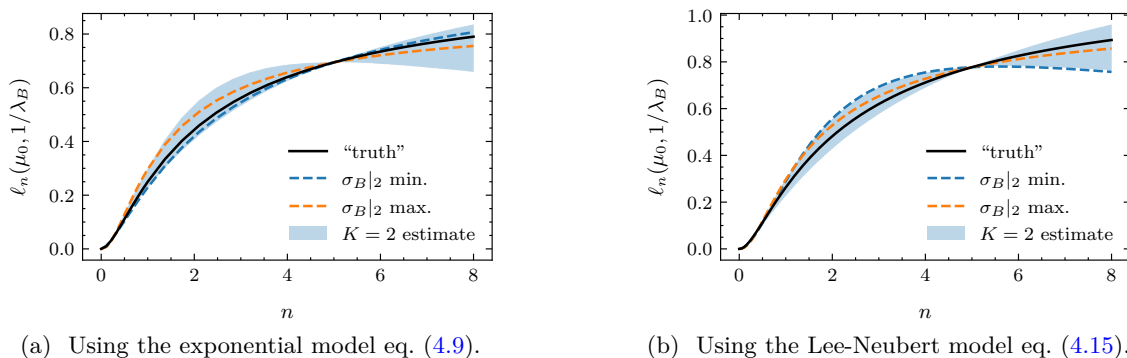


Figure 7. Pseudo-fit to the normalized Laplace transform $\ell_n(\mu_0, 1/\lambda_B)$ using the two pseudo-observables $p_{1,2}$ as predicted by two models as a function of $x = \omega/\lambda_B$. We show the model (“truth”), the curves that lead to extreme values of σ_B and the total variation of the parametrized LCDA. For the latter, we take the benchmark interval for $\xi = \omega_0/\lambda_B$ and a small a_2 into account.

5.1.1 Exponential model

In the exponential model eq. (4.9) the value for the pseudo-observable p_2 is given by

$$p_2 = \frac{25}{36} \simeq 0.694, \quad [\text{exp. model}] \quad (5.5)$$

from which we can directly determine the coefficients a_0 and a_1 in the truncated parametrization. We may now determine the maximal range of values that σ_B can take, when the free parameters ξ and a_2 are varied as explained above. This results in

$$\sigma_B|_2^{\min} = -0.073 \quad \text{for } \xi \rightarrow 1.332 \text{ and } a_2 \rightarrow +0.410, \quad (5.6)$$

$$\sigma_B|_2^{\max} = +0.172 \quad \text{for } \xi \rightarrow 1.489 \text{ and } a_2 \rightarrow -0.625, \quad (5.7)$$

while $\sigma_B = 0$ in the exponential model. We further plot the momentum space LCDA $\phi_+(\omega, \mu_0)$ and its corresponding Laplace transform $\ell_n(\mu_0, 1/\lambda_B)$ in figure 6a and figure 7a, respectively, as well as the corresponding curves for the extreme values of σ_B . We find that the parameter values are constrained to the intervals $0.607 < \xi < 1.499$, $-0.633 < a_2 < 0.477$, and $0.607 < \xi < 1.636$, $-0.632 < a_2 < 0.539$, respectively. We observe the following:

1. The knowledge of the pseudo-observables p_1 and p_2 indeed fixes the behavior of $\phi_+(\omega)$ at low momentum, as well as the behavior of its Laplace transform at large values of $\zeta = -i\tau \gg \lambda_B$.
2. The shape of $\phi_+(\omega)$ at intermediate values of ω is very sensitive to the variation of ξ and a_2 , and therefore not very meaningful without additional phenomenological constraints.
3. Similarly, the behavior of the Laplace transform at small values of $\zeta \lesssim 1$ is sensitive to the variation of ξ and a_2 , but in contrast to the LCDA in momentum space, the shape of the Laplace transform remains stable, reflecting a monotonous function (at least, as long as ζ is not too close to zero).

From this we can already see, that a meaningful fit to the LCDA would benefit from additional information on the Laplace transform at small values of ζ (i.e. the LCDA in position space at imaginary light-cone time $-i\tau \lesssim \lambda_B$). This will be further illustrated below.

5.1.2 Lee-Neubert model with radiative tail

In the Lee-Neubert model eq. (4.15) the value for the pseudo-observable p_2 is given by

$$p_2 \simeq 0.777 \quad [\text{Lee/Neubert}], \quad (5.8)$$

which is slightly larger than for the exponential model. The corresponding ranges for the logarithmic moment are obtained as

$$\sigma_B|_2^{\min} = 0.045 \quad \text{for } \xi \rightarrow 0.541 \text{ and } a_2 \rightarrow -0.225, \quad (5.9)$$

$$\sigma_B|_2^{\max} = 0.321 \quad \text{for } \xi \rightarrow 1.283 \text{ and } a_2 \rightarrow -0.543. \quad (5.10)$$

This includes the value $\sigma_B \simeq 0.315$ of the LN model. We observe that values of p_2 that are larger than in the exponential model yield larger values of σ_B . We will discuss how to consistently implement information on the “radiative tail” in a modified fit procedure in section 5.2. We plot the momentum-space LCDA and its Laplace transform in figure 6b and figure 7b. We find that the parameter values are constrained to the intervals $0.498 < \xi < 1.342$, $-0.546 < a_2 < 0.439$, and $0.540 < \xi < 1.381$, $-0.536 < a_2 < 0.458$, respectively.

5.1.3 Naïve parton model

We can repeat the analysis for the naïve parton model. Here the pseudo-observable p_2 takes the value

$$p_2 = (1 - 11 e^{-10})/2 \simeq 0.5 \quad [\text{parton model}], \quad (5.11)$$

which now is *smaller* than in the exponential model. With this, the range of values that σ_B can take amounts to

$$\sigma_B|_2^{\min} = -0.565 \quad \text{for } \xi \rightarrow 1.810 \text{ and } a_2 \rightarrow +0.543, \quad (5.12)$$

$$\sigma_B|_2^{\max} = -0.231 \quad \text{for } \xi \rightarrow 2.228 \text{ and } a_2 \rightarrow -0.943, \quad (5.13)$$

which includes the “true” value $\sigma_B \simeq -0.270$ in the naïve parton model. We find that the parameter values are constrained to the intervals $0.824 < \xi < 2.229$, $-0.948 < a_2 < 0.536$, and $0.824 < \xi < 2.242$, $-0.947 < a_2 < 0.697$, respectively. Qualitatively, as before, we observe that now smaller values of p_2 tend to yield smaller values of σ_B in the pseudo-fit.

5.1.4 Model with $\phi'_+(\mathbf{0}) \rightarrow \infty$

Repeating the analysis for the model eq. (4.22), we observe that the value of the pseudo-observable

$$p_2 \simeq 0.701 \quad [\text{Beneke et al.}] \quad (5.14)$$

is very close to that of the exponential model. As a consequence — without further input — the fit cannot distinguish the two cases. Note that the range for the first logarithmic moment that results from our fit procedure will not include the actual value $\sigma_B = 0.453$ in this model. This can be traced back to the pathological behavior of the model at $\omega \rightarrow 0$.

5.2 Adding theoretical constraints from the short-distance OPE

As has previously been mentioned, the B -meson LCDA can be constrained using information obtained from the short-distance OPE of the light-cone operator. The latter describes the behavior of $\tilde{\phi}_+(\tau)$ at small values of $|\tau| \sim 1/\mu \ll 1/\Lambda_{\text{QCD}}$, and it can be obtained from a fixed-order partonic calculation in HQET [25],

$$\tilde{\phi}_+(\tau, \mu) = 1 - \frac{\alpha_s C_F}{4\pi} \left(2L^2 + 2L + \frac{5\pi^2}{12} \right) - i\tau \frac{4\bar{\Lambda}}{3} \left[1 - \frac{\alpha_s C_F}{4\pi} \left(2L^2 + 4L - \frac{9}{4} + \frac{5\pi^2}{12} \right) \right] + \mathcal{O}(\tau^2 \Lambda_{\text{QCD}}^2). \quad (5.15)$$

In the above, $\bar{\Lambda}$ is the HQET mass parameter in the on-shell scheme and we abbreviate

$$L = \ln(i\tau\mu e^{\gamma_E}).$$

In the Lee-Neubert model eq. (4.15) the short-distance information has been added as a radiative tail in momentum space, by considering cut-off moments $M_n(\Lambda_{\text{UV}}) = \int_0^{\Lambda_{\text{UV}}} d\omega \omega^n \phi_+(\omega)$. A more direct and simpler approach is to evaluate the LCDA in position space, using our parametrization, and compare with eq. (5.15). To this end, we have to first expand our parametrization in $\omega_0/\mu_0 \ll 1$ for a fixed value of

$$x_0 \equiv i\tau_0\mu_0 e^{\gamma_E} \sim \mathcal{O}(1) \quad (5.16)$$

The analogue of the first two moments M_0 and M_1 used in the Lee-Neubert model are then taken as the value and first derivative of $\tilde{\phi}_+(\tau)$, which defines the two theory inputs

$$t_1 \equiv \tilde{\phi}(\tau_0, \mu_0), \quad t_2 \equiv i \frac{d\tilde{\phi}(\tau, \mu_0)}{d\tau} \Big|_{\tau=\tau_0}. \quad (5.17)$$

Let us first consider a situation where only this theory input is known. A minimal approach would then be to consider our parametrization at truncation level $K = 1$ and fix the parameters a_0 and a_1 by matching t_1 and t_2 to eq. (5.15). This yields

$$a_0 = 2 - \frac{2\bar{\Lambda}}{3\omega_0} + \frac{\alpha_s C_F}{4\pi} \left(-\frac{1}{x_0} \frac{\mu_0 e^{\gamma_E}}{\omega_0} (1 + 2 \ln x_0) + \dots \right), \quad (5.18)$$

$$a_1 = 1 - \frac{2\bar{\Lambda}}{3\omega_0} + \frac{\alpha_s C_F}{4\pi} \left(-\frac{1}{x_0} \frac{\mu_0 e^{\gamma_E}}{\omega_0} (1 + 2 \ln x_0) + \dots \right), \quad (5.19)$$

where we only show the α_s corrections that are enhanced by μ_0/ω_0 . These terms can be absorbed by a redefinition of the HQET mass parameter: for our purpose, a convenient renormalization scheme is⁷

$$\bar{\Lambda} \equiv \bar{\Lambda}_a(\mu, x_0) \left[1 + \frac{\alpha_s C_F}{4\pi} \left(10 \ln x_0 + \frac{15}{4} \right) \right] - \frac{\alpha_s C_F}{4\pi} \frac{3\mu e^{\gamma_E}}{2x_0} (1 + 2 \ln x_0) \quad (5.20)$$

⁷A similar definition has been derived from the analysis of the cut-off moments M_0 and M_1 in ref. [12], leading to the above-mentioned “DA-scheme” for the HQET mass parameter.

which yields

$$a_0 = Z(x_0) \left(2 - \frac{2\bar{\Lambda}_a}{3\omega_0} - \frac{8\alpha_s C_F}{3\pi} \frac{\bar{\Lambda}_a x_0}{\mu_0 e^{\gamma_E}} (1 + \ln x_0) \right), \quad (5.21)$$

$$a_1 = Z(x_0) \left(1 - \frac{2\bar{\Lambda}_a}{3\omega_0} - \frac{4\alpha_s C_F}{3\pi} \frac{\bar{\Lambda}_a x_0}{\mu_0 e^{\gamma_E}} (1 + \ln x_0) \right), \quad (5.22)$$

with

$$Z(x_0) = 1 + \frac{\alpha_s C_F}{4\pi} \left(-2 \ln^2 x_0 + 2 \ln x_0 + 2 - \frac{5\pi^2}{12} \right). \quad (5.23)$$

Our definition of $\bar{\Lambda}_a$ and $Z(x_0)$ have been chosen such that the result for the position-space LCDA with finite truncation K always satisfies

$$\begin{aligned} \tilde{\phi}_+(0)|_K &= \sum_{k=1}^K (-1)^k a_k = Z(x_0) - \frac{4\alpha_s C_F}{3\pi} \frac{\bar{\Lambda}_a x_0}{\mu_0 e^{\gamma_E}} (1 + \ln x_0), \\ \tilde{\phi}'_+(0)|_K &= -2i\omega_0 \sum_{k=1}^K (-1)^k (1+k) a_k = -Z(x_0) \frac{4i\bar{\Lambda}_a}{3}, \end{aligned} \quad (5.24)$$

which generalizes the Grozin-Neubert relations in ref. [11] to one-loop accuracy in our formalism.⁸ It is instructive to compare with the approach by Lee and Neubert in ref. [12], where corresponding expressions are obtained for the zeroth and first moment of the momentum-space LCDA with a UV cut off. The perturbative relation between the parameter $\bar{\Lambda}_{\text{DA}}$ defined in that scheme and our scheme reads

$$\bar{\Lambda}_a(\mu, x_0) = \bar{\Lambda}_{\text{DA}}(\mu, \mu) \left[1 + \frac{\alpha_s C_F}{4\pi} (-10 \ln x_0 - 2) \right] + \mu \frac{\alpha_s C_F}{4\pi} \left(\frac{3e^{\gamma_E}}{2x_0} (1 + 2 \ln x_0) - \frac{9}{2} \right). \quad (5.25)$$

For instance, using $x_0 = 1$, $\mu_0 = 1 \text{ GeV}$, $\bar{\Lambda}_{\text{DA}}(\mu_0, \mu_0) = 519 \text{ MeV}$, and $\alpha_s(\mu_0) = 0.5$ as in ref. [12], we obtain

$$\bar{\Lambda}_a(\mu_0, x_0) = 367 \text{ MeV}.$$

We are now in the position to include the phenomenological constraints p_1 and p_2 as defined in the previous subsection. For the sake of legibility, we introduce the quantity

$$n_0 \equiv i\tau_0\omega_0 = \frac{x_0\omega_0}{\mu_0 e^{\gamma_E}}. \quad (5.26)$$

For the power expansion defined by the OPE to converge, we would need $x_0 \sim \mathcal{O}(1)$ and small values of n_0 . On the other hand, the (reasonably fast) convergence of our parametrization requires a finite $n_0 > 0$. In the following, we use

$$n_0 = 1/3, \quad \mu_0 = 1 \text{ GeV},$$

⁸The conditions eq. (5.24) take the same form in dual space, since $\eta_+(0) = \tilde{\phi}_+(0)$ and $\eta'_+(0) = -\frac{i}{2} \tilde{\phi}'_+(0)$ for finite truncation K .

as our default choice, while the value of ω_0 (and thus of x_0) will be varied within the fit, with suitable constraints on the resulting relative growth (see below). For instance, a value $x_0 = 1$ corresponds to $\omega_0 \approx 600$ MeV, which appears reasonable. Note that our choice for n_0 corresponds to the value $y_0 = -1/2$ in eq. (3.2), which lies exactly halfway between the origin and the local limit ($y = -1$).

With two new constraints we increase the truncation level from $K = 2 \rightarrow 4$ compared to the previous subsection, leaving $a_4(\mu_0)$ and $\xi = \omega_0/\lambda_B$ as free parameters. For $\xi = 1$ and $x_0 = 1$ we obtain

$$a_0 = Z \left(-\frac{28}{25} + \frac{2\bar{\Lambda}_a p_1}{15} \right) + \frac{112\alpha_s C_F}{75\pi} \bar{\Lambda}_a n_0 p_1 + 3 - \frac{972 p_2}{625} - \frac{4a_4}{15}, \quad (5.27)$$

$$a_1 = Z \left(-2 + \frac{\bar{\Lambda}_a p_1}{3} \right) + \frac{8\alpha_s C_F}{3\pi} \bar{\Lambda}_a n_0 p_1 + \frac{3}{2} - \frac{4a_4}{5}, \quad (5.28)$$

$$a_2 = Z \left(\frac{84}{25} - \frac{2\bar{\Lambda}_a p_1}{5} \right) - \frac{112\alpha_s C_F}{25\pi} \bar{\Lambda}_a n_0 p_1 - 6 + \frac{2916 p_2}{625} + \frac{a_4}{5}, \quad (5.29)$$

$$a_3 = Z \left(\frac{81}{25} - \frac{3\bar{\Lambda}_a p_1}{5} \right) - \frac{108\alpha_s C_F}{25\pi} \bar{\Lambda}_a n_0 p_1 - \frac{9}{2} + \frac{1944 p_2}{625} + \frac{26a_4}{15}, \quad (5.30)$$

where $Z \equiv Z(x_0 = 1)$. The result for arbitrary values of ξ and x_0 can be found in appendix B. The parameter range for a_4 and ξ will be further constrained by analogous conditions on the relative growth as in the previous subsection,

$$\text{Gr}[\chi]_K \leq \frac{20\%}{K} \quad (5.31)$$

which generalizes eq. (5.3).

Among the four benchmark models discussed in section 4, only the Lee-Neubert model in eq. (4.15) features a radiative tail that reflects the constraints from the local OPE. We therefore consider this model as a benchmark. We expect that the pseudo-fit should correctly reproduce the main qualitative and quantitative features of that model. We therefore set

$$p_1 = 1/\lambda_B = 2.085 \text{ GeV}^{-1}, \quad p_2 = 0.777 \quad [\text{Lee/Neubert}], \quad (5.32)$$

and take the same input for the theory parameters as outlined below eq. (4.15), while $\bar{\Lambda}_a$ is calculated from eq. (5.25) as a function of x_0 . As in section 5, we consider the normalized first logarithmic moment, now truncated at $K = 4$,

$$\sigma_B|_4 = -\ln \xi + \frac{a_1 + 2/3 a_3}{\xi}. \quad (5.33)$$

We find the following range of values, constrained by the growth criterion,

$$\sigma_B|_4^{\min} = 0.114 \quad \text{for } \xi \rightarrow 0.961 \text{ and } a_2 \rightarrow -0.232, \quad (5.34)$$

$$\sigma_B|_4^{\max} = 0.217 \quad \text{for } \xi \rightarrow 0.905 \text{ and } a_2 \rightarrow -0.030. \quad (5.35)$$

This interval is compatible with the estimate obtained by using only p_1 and p_2 . However, its size is reduced by more than 60%. The value $\sigma_B = 0.315$ in the Lee/Neubert model is not contained in this estimate.

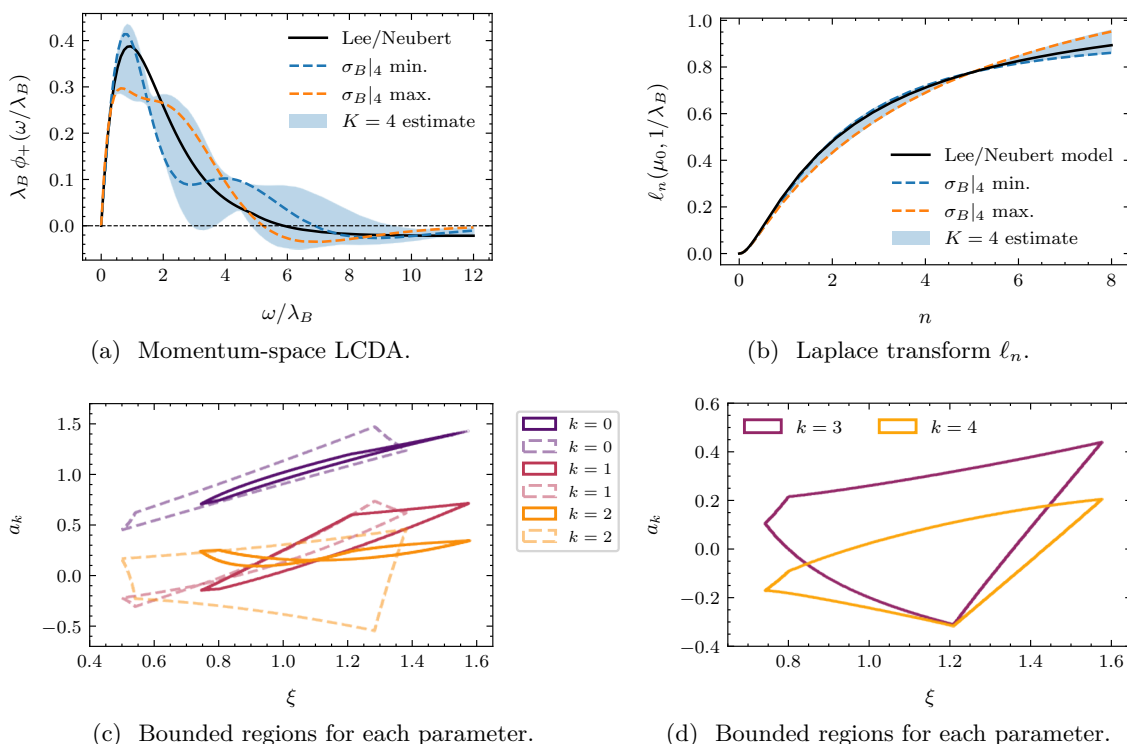


Figure 8. Results from the pseudo-fit employing theoretical constraints in addition to the phenomenological inputs p_1 and p_2 . The dashed regions in figure 8c correspond to the pseudo-fit *without* theoretical OPE constraints.

We show the resulting momentum-space LCDA and Laplace transform in figure 8a and figure 8b, respectively, where we find that the parameters are restricted as $0.745 < \xi < 1.577$, $-0.319 < a_4 < 0.201$, and $0.743 < \xi < 1.522$, $-0.312 < a_4 < 0.120$. In figure 8c, we compare the allowed regions for the coefficients a_0 through a_2 obtained here with the ones as obtained in section 5. We find that the regions largely overlap, while shrinking significantly for a_0 and a_2 and staying approximately constant for a_1 . We further show the regions for the additional coefficients a_3 and a_4 in figure 8d.

Once more, we caution that the plots and numerical results here illustrate the applicability of our method. However, they cannot be interpreted as predictions, which would require a more careful treatment of uncertainties on the basis of experimental data.

6 Conclusion and outlook

We have proposed a novel systematic parametrization of the leading-twist B -meson light-cone distribution amplitude (LCDA) in position space. At the center of our derivation is the Taylor expansion of the LCDA in a conveniently chosen variable y , which arises from the conformal transformation in eq. (3.2). The coefficients of that expansion obey an integral bound eq. (3.8), which provides qualitative control of the truncation error of the expansion, with the numerical value of the bound presently unknown. Our parametrization yields simple expressions for a variety of quantities connected to the LCDA, including its logarithmic moments and a set of “pseudo-observables” describing the low-momentum

behavior. For convenience we summarize the resulting formulas for the most important functions in table 1. We have also discussed three different approaches to implement the renormalization-group (RG) evolution of the LCDA and its derived quantities within our framework. We have identified one approach that allows a computationally efficient implementation in future phenomenological analyses.

We have performed detailed numerical studies to show that our parametrization can successfully reproduce different benchmark models, including non-trivial features like the “radiative tail” at large light-cone momentum. Furthermore, we have illustrated the power of our approach to combine different types of phenomenological and theoretical constraints. This is achieved through matching our parametrization to hypothetical values of two “pseudo-observables” in eq. (5.1) that are expected to be constrained by future experimental data on the photo-leptonic $B \rightarrow \gamma \ell \nu$ decay. Moreover, we have shown that theoretical constraints on the expansion parameters from the local operator product expansion (OPE) can be implemented at small but finite light-cone separation in a natural and straightforward manner. We have used this to define a new renormalization scheme eq. (5.20) for the mass parameter in heavy-quark effective theory (HQET), which resembles the so-called “DA-scheme” that has been introduced by Lee and Neubert from the consideration of “cut-off” moments.

Our framework is general enough to allow theoretical refinements in the future. First, it can be applied to higher-twist LCDA of the B -meson, as we have briefly discussed for the Wandzura-Wilczek part of the twist-three LCDA ϕ_- . Second, the available two-loop RG evolution can be implemented on the level of our truncated expansion. Third, the OPE constraints from dimension-five HQET operators can be included as well. Finally, on the phenomenological side, a future determination of the very value of the integral bound, e.g. from lattice QCD studies, would allow us to quantify the truncation errors.

Note Added. During the final phase of this work, ref. [32] appeared. Among others, it discusses a complementary approach to parametrizing the leading B -meson LCDA, where the generating function eq. (2.15) is expanded in t . The logarithmic moments appear as the expansion coefficients. In contrast to our work, this expansion is not controlled by an integral bound.

Acknowledgments

We thank Guido Bell, Martin Beneke, and Björn O. Lange for helpful discussions. T.F. would like to thank Roman Zwicky for discussions about the B -meson LCDA, which initiated some of the ideas presented in this work. The research of T.F. is supported by the Deutsche Forschungsgemeinschaft (DFG, German Research Foundation) under grant 396021762 — TRR 257. The work of D.v.D. is supported by the DFG within the Emmy Noether Programme under grant DY-130/1-1 and the Sino-German Collaborative Research Center TRR110 “Symmetries and the Emergence of Structure in QCD” (DFG Project-ID 196253076, NSFC Grant No. 12070131001, TRR 110). P.L. and D.v.D. were supported in the final phase of this work by the Munich Institute for Astro- and Particle Physics (MIAPP), which is funded by the DFG under Germany’s Excellence Strategy — EXC-2094 — 390783311.

position-space LCDA	$\tilde{\phi}_+(\tau, \mu_0) = \frac{1}{(1+i\omega_0\tau)^2} \sum_{k=0}^K a_k(\mu_0) \left(\frac{i\omega_0\tau-1}{i\omega_0\tau+1}\right)^k$
momentum-space LCDA	$\phi_+(\omega, \mu_0) = \frac{\omega e^{-\omega/\omega_0}}{\omega_0^2} \sum_{k=0}^K a_k(\mu_0) \frac{1}{1+k} L_k^{(1)}(2\omega/\omega_0)$
dual-space LCDA	$\eta_+(s, \mu_0) = e^{-s\omega_0} \sum_{k=0}^K a_k(\mu_0) \frac{(-1)^k}{1+k} L_k^{(1)}(2\omega_0 s)$
generating function	$F_{[\eta_+]}(t; \mu_0, \mu_m) = \frac{\Gamma(1-t)}{\omega_0} \left(\frac{\mu_m}{\omega_0}\right)^{-t} \sum_{k=0}^K a_k(\mu_0) {}_2F_1(-k, 1+t; 2, 2)$
inverse moment	$\lambda_B^{-1}(\mu_0) = \frac{1}{\omega_0} \sum_{k=0}^K a_k(\mu_0) \frac{1+(-1)^k}{2(1+k)} \quad (\text{only even } k)$
logarithmic moment	$\sigma_B(\mu_0) = -\ln \xi - \frac{1}{\xi} \sum_{k=0}^K a_k(\mu_0) \left[\frac{d}{dt} {}_2F_1(-k, 1+t; 2; 2)\right]_{t=0} \quad (\text{only odd } k)$
derivative at $\omega = 0$	$\phi'_+(0, \mu_0) = \frac{1}{\omega_0^2} \sum_{k=0}^K a_k(\mu_0)$

Table 1. Summary of representations and pseudo observables connected to the leading-twist B -meson LCDA within our proposed parametrization at the low-energy reference scale μ_0 . Here $L_k^{(1)}$ are associated Laguerre polynomials, and $\xi = \omega_0/\lambda_B$.

A Useful definitions and formulas

Our definition of the RG functions $V(\mu; \mu_0)$ and $g(\mu; \mu_0)$ reads (see e.g. ref. [33]),

$$V(\mu, \mu_0) = - \int_{\alpha_s(\mu_0)}^{\alpha_s(\mu)} \frac{d\alpha}{\beta(\alpha)} \left[\gamma_+(\alpha) + \Gamma_c(\alpha) \int_{\alpha_s(\mu_0)}^{\alpha} \frac{d\alpha}{\beta(\alpha)} \right], \quad (\text{A.1})$$

$$g(\mu; \mu_0) = \int_{\alpha_s(\mu_0)}^{\alpha_s(\mu)} \frac{d\alpha}{\beta(\alpha)} \Gamma_c(\alpha). \quad (\text{A.2})$$

A useful relation for Bessel functions reads (see e.g. ref. [22])

$$\int_0^\infty d\omega e^{-i\omega z} \left(\frac{\omega}{s}\right)^{j-1/2} J_{2j-1}(2\sqrt{s\omega}) = e^{-i\pi j} \frac{e^{is/z}}{z^{2j}}. \quad (\text{A.3})$$

Furthermore, Bessel functions can be expanded as an infinite series of associated Laguerre polynomials,

$$J_\alpha(x) = \left(\frac{x}{2}\right)^\alpha \frac{e^{-t}}{\Gamma(1+\alpha)} \sum_{k=0}^\infty \frac{\alpha!}{(k+\alpha)!} L_k^{(\alpha)}\left(\frac{x^2}{4t}\right) t^k, \quad (\text{A.4})$$

with an arbitrary parameter t . Especially, using $t = \omega/\omega_0$, one gets

$$J_1(2\sqrt{\omega s}) = \sqrt{\omega s} e^{-\omega/\omega_0} \sum_{k=0}^\infty \frac{1}{(1+k)!} L_k^{(1)}(s\omega_0) \left(\frac{\omega}{\omega_0}\right)^k. \quad (\text{A.5})$$

We list useful relations involving the associated Laguerre polynomials for the readers convenience. The polynomials can be written in closed form,

$$L_n^{(\alpha)}(x) = \sum_{i=0}^n (-1)^i \binom{n+\alpha}{n-i} \frac{x^i}{i!}. \quad (\text{A.6})$$

We list the first four orders for $\alpha = 1$:

$$L_0^{(1)} = 1, \quad L_1^{(1)} = -x + 2, \quad L_2^{(1)} = \frac{1}{2}(x^2 - 6x + 6), \quad L_3^{(1)} = \frac{1}{6}(-x^3 + 12x^2 - 36x + 24). \quad (\text{A.7})$$

They fulfill the following orthogonality relation:

$$\int_0^\infty dx x^\alpha e^{-x} L_n^{(\alpha)}(x) L_m^{(\alpha)}(x) = \frac{\Gamma(n + \alpha + 1)}{n!} \delta_{nm}. \quad (\text{A.8})$$

They can be obtained as the Taylor coefficients of the series

$$\sum_{n=0}^\infty t^n L_n^{(\alpha)}(x) = \frac{1}{(1-t)^{\alpha+1}} e^{-tx/(1-t)}. \quad (\text{A.9})$$

B Solutions for expansion coefficients a_k from pseudo-phenomenology and OPE

The solutions for the expansion coefficients a_{0-3} with the constraints from the pseudo-observables p_1 and p_2 and the two theory inputs t_1 and t_2 (see section 5) for arbitrary values of ξ , x_0 , n_0 and a_4 are given by

$$a_0 = Z \left(-\frac{(5\xi - 1)(1 + 30\xi + 25\xi^2)}{100\xi^2(5\xi - 3)} + \frac{5\xi - 1}{15\xi^2(5\xi - 3)} \bar{\Lambda}_a p_1 \right) + \frac{3\xi(5\xi - 1)}{2(5\xi - 3)} - \frac{(5\xi + 1)^5}{2500\xi^2(5\xi - 3)} p_2 - \frac{(9 - 5\xi)(5\xi - 1)}{5(5\xi - 3)(5\xi + 1)} a_4 + \frac{(5\xi - 1)(1 + 30\xi + 25\xi^2) \alpha_s C_F}{75\pi\xi^3(5\xi - 3)} \bar{\Lambda}_a n_0 p_1 (1 + \ln x_0), \quad (\text{B.1})$$

$$a_1 = Z \left(-2 + \frac{1}{3\xi} \bar{\Lambda}_a p_1 \right) + \frac{3\xi}{2} + \frac{8\alpha_s C_F}{3\pi} \frac{\bar{\Lambda}_a n_0}{\xi} (1 + \ln x_0) p_1 - \frac{4a_4}{5}, \quad (\text{B.2})$$

$$a_2 = Z \left(\frac{3(5\xi - 1)(1 + 30\xi + 25\xi^2)}{100\xi^2(5\xi - 3)} - \frac{5\xi - 1}{5\xi^2(5\xi - 3)} \bar{\Lambda}_a p_1 \right) - \frac{3\xi(5\xi + 3)}{2(5\xi - 3)} + \frac{3(5\xi + 1)^5}{2500\xi^2(5\xi - 3)} p_2 + \frac{6(-3 + 30\xi - 25\xi^2)}{5(5\xi - 3)(5\xi + 1)} a_4 - \frac{(5\xi - 1)(1 + 30\xi + 25\xi^2) \alpha_s C_F}{25\pi\xi^3(5\xi - 3)} \bar{\Lambda}_a n_0 p_1 (1 + \ln x_0), \quad (\text{B.3})$$

$$a_3 = Z \left(\frac{(5\xi + 1)(-1 - 20\xi + 75\xi^2)}{50\xi^2(5\xi - 3)} - \frac{(5\xi - 2)(5\xi + 1)}{15\xi^2(5\xi - 3)} \bar{\Lambda}_a p_1 \right) - \frac{3\xi(5\xi + 1)}{2(5\xi - 3)} + \frac{(5\xi + 1)^5}{1250\xi^2(5\xi - 3)} p_2 + \frac{4(-9 + 10\xi + 25\xi^2)}{5(5\xi - 3)(5\xi + 1)} a_4 - \frac{2(5\xi + 1)(-1 - 20\xi + 75\xi^2) \alpha_s C_F}{75\pi\xi^3(5\xi - 3)} \bar{\Lambda}_a n_0 p_1 (1 + \ln x_0). \quad (\text{B.4})$$

Open Access. This article is distributed under the terms of the Creative Commons Attribution License ([CC-BY 4.0](https://creativecommons.org/licenses/by/4.0/)), which permits any use, distribution and reproduction in any medium, provided the original author(s) and source are credited. SCOAP³ supports the goals of the International Year of Basic Sciences for Sustainable Development.

References

- [1] M. Beneke, G. Buchalla, M. Neubert and C.T. Sachrajda, *QCD factorization for $B \rightarrow \pi\pi$ decays: Strong phases and CP-violation in the heavy quark limit*, *Phys. Rev. Lett.* **83** (1999) 1914 [[hep-ph/9905312](https://arxiv.org/abs/hep-ph/9905312)] [[INSPIRE](https://inspirehep.net/literature/252701)].
- [2] M. Beneke, G. Buchalla, M. Neubert and C.T. Sachrajda, *QCD factorization in $B \rightarrow \pi K, \pi\pi$ decays and extraction of Wolfenstein parameters*, *Nucl. Phys. B* **606** (2001) 245 [[hep-ph/0104110](https://arxiv.org/abs/hep-ph/0104110)] [[INSPIRE](https://inspirehep.net/literature/280001)].
- [3] BELLE-II collaboration, *The Belle II Physics Book*, *PTEP* **2019** (2019) 123C01 [Erratum *ibid.* **2020** (2020) 029201] [[arXiv:1808.10567](https://arxiv.org/abs/1808.10567)] [[INSPIRE](https://inspirehep.net/literature/163171)].
- [4] A. Khodjamirian, T. Mannel and N. Offen, *B-meson distribution amplitude from the $B \rightarrow \pi$ form-factor*, *Phys. Lett. B* **620** (2005) 52 [[hep-ph/0504091](https://arxiv.org/abs/hep-ph/0504091)] [[INSPIRE](https://inspirehep.net/literature/43311)].
- [5] F. De Fazio, T. Feldmann and T. Hurth, *Light-cone sum rules in soft-collinear effective theory*, *Nucl. Phys. B* **733** (2006) 1 [Erratum *ibid.* **800** (2008) 405] [[hep-ph/0504088](https://arxiv.org/abs/hep-ph/0504088)] [[INSPIRE](https://inspirehep.net/literature/114001)].
- [6] A. Khodjamirian, T. Mannel and N. Offen, *Form-factors from light-cone sum rules with B-meson distribution amplitudes*, *Phys. Rev. D* **75** (2007) 054013 [[hep-ph/0611193](https://arxiv.org/abs/hep-ph/0611193)] [[INSPIRE](https://inspirehep.net/literature/141001)].
- [7] F. De Fazio, T. Feldmann and T. Hurth, *SCET sum rules for $B \rightarrow P$ and $B \rightarrow V$ transition form factors*, *JHEP* **02** (2008) 031 [[arXiv:0711.3999](https://arxiv.org/abs/hep-ph/0711.3999)] [[INSPIRE](https://inspirehep.net/literature/150001)].
- [8] M. Beneke and J. Rohrwild, *B meson distribution amplitude from $B \rightarrow \gamma\ell\nu$* , *Eur. Phys. J. C* **71** (2011) 1818 [[arXiv:1110.3228](https://arxiv.org/abs/hep-ph/1110.3228)] [[INSPIRE](https://inspirehep.net/literature/100001)].
- [9] V.M. Braun and A. Khodjamirian, *Soft contribution to $B \rightarrow \gamma\ell\nu_\ell$ and the B-meson distribution amplitude*, *Phys. Lett. B* **718** (2013) 1014 [[arXiv:1210.4453](https://arxiv.org/abs/hep-ph/1210.4453)] [[INSPIRE](https://inspirehep.net/literature/110001)].
- [10] M. Beneke, V.M. Braun, Y. Ji and Y.-B. Wei, *Radiative leptonic decay $B \rightarrow \gamma\ell\nu_\ell$ with subleading power corrections*, *JHEP* **07** (2018) 154 [[arXiv:1804.04962](https://arxiv.org/abs/hep-ph/1804.04962)] [[INSPIRE](https://inspirehep.net/literature/150001)].
- [11] A.G. Grozin and M. Neubert, *Asymptotics of heavy meson form-factors*, *Phys. Rev. D* **55** (1997) 272 [[hep-ph/9607366](https://arxiv.org/abs/hep-ph/9607366)] [[INSPIRE](https://inspirehep.net/literature/43311)].
- [12] S.J. Lee and M. Neubert, *Model-independent properties of the B-meson distribution amplitude*, *Phys. Rev. D* **72** (2005) 094028 [[hep-ph/0509350](https://arxiv.org/abs/hep-ph/0509350)] [[INSPIRE](https://inspirehep.net/literature/114001)].
- [13] B.O. Lange and M. Neubert, *Renormalization group evolution of the B meson light cone distribution amplitude*, *Phys. Rev. Lett.* **91** (2003) 102001 [[hep-ph/0303082](https://arxiv.org/abs/hep-ph/0303082)] [[INSPIRE](https://inspirehep.net/literature/100001)].
- [14] G. Bell, T. Feldmann, Y.-M. Wang and M.W.Y. Yip, *Light-Cone Distribution Amplitudes for Heavy-Quark Hadrons*, *JHEP* **11** (2013) 191 [[arXiv:1308.6114](https://arxiv.org/abs/hep-ph/1308.6114)] [[INSPIRE](https://inspirehep.net/literature/110001)].
- [15] V.M. Braun and A.N. Manashov, *Conformal symmetry of the Lange-Neubert evolution equation*, *Phys. Lett. B* **731** (2014) 316 [[arXiv:1402.5822](https://arxiv.org/abs/hep-ph/1402.5822)] [[INSPIRE](https://inspirehep.net/literature/120001)].
- [16] V.M. Braun, Y. Ji and A.N. Manashov, *Two-loop evolution equation for the B-meson distribution amplitude*, *Phys. Rev. D* **100** (2019) 014023 [[arXiv:1905.04498](https://arxiv.org/abs/hep-ph/1905.04498)] [[INSPIRE](https://inspirehep.net/literature/170001)].

- [17] Z.L. Liu, B. Mecaj, M. Neubert, X. Wang and S. Fleming, *Renormalization and Scale Evolution of the Soft-Quark Soft Function*, *JHEP* **07** (2020) 104 [[arXiv:2005.03013](#)] [[INSPIRE](#)].
- [18] A.M. Galda and M. Neubert, *Evolution of the B-Meson Light-Cone Distribution Amplitude in Laplace Space*, *Phys. Rev. D* **102** (2020) 071501 [[arXiv:2006.05428](#)] [[INSPIRE](#)].
- [19] V.M. Braun, D.Y. Ivanov and G.P. Korchemsky, *The B meson distribution amplitude in QCD*, *Phys. Rev. D* **69** (2004) 034014 [[hep-ph/0309330](#)] [[INSPIRE](#)].
- [20] A.G. Grozin and G.P. Korchemsky, *Renormalized sum rules for structure functions of heavy mesons decays*, *Phys. Rev. D* **53** (1996) 1378 [[hep-ph/9411323](#)] [[INSPIRE](#)].
- [21] R.S. Strichartz, *A Guide To Distribution Theory And Fourier Transforms*, CRC Press (2003) [[DOI](#)].
- [22] V.M. Braun, Y. Ji and A.N. Manashov, *Higher-twist B-meson Distribution Amplitudes in HQET*, *JHEP* **05** (2017) 022 [[arXiv:1703.02446](#)] [[INSPIRE](#)].
- [23] T. Feldmann, B.O. Lange and Y.-M. Wang, *B -meson light-cone distribution amplitude: Perturbative constraints and asymptotic behavior in dual space*, *Phys. Rev. D* **89** (2014) 114001 [[arXiv:1404.1343](#)] [[INSPIRE](#)].
- [24] I. Caprini, *Functional Analysis and Optimization Methods in Hadron Physics*, SpringerBriefs in Physics, Springer (2019) [[DOI](#)] [[INSPIRE](#)].
- [25] H. Kawamura and K. Tanaka, *Operator product expansion for B-meson distribution amplitude and dimension-5 HQET operators*, *Phys. Lett. B* **673** (2009) 201 [[arXiv:0810.5628](#)] [[INSPIRE](#)].
- [26] H. Kawamura, J. Kodaira, C.-F. Qiao and K. Tanaka, *B-meson light cone distribution amplitudes in the heavy quark limit*, *Phys. Lett. B* **523** (2001) 111 [*Erratum ibid.* **536** (2002) 344] [[hep-ph/0109181](#)] [[INSPIRE](#)].
- [27] S. Descotes-Genon and N. Offen, *Three-particle contributions to the renormalisation of B-meson light-cone distribution amplitudes*, *JHEP* **05** (2009) 091 [[arXiv:0903.0790](#)] [[INSPIRE](#)].
- [28] G. Bell and T. Feldmann, *Modelling light-cone distribution amplitudes from non-relativistic bound states*, *JHEP* **04** (2008) 061 [[arXiv:0802.2221](#)] [[INSPIRE](#)].
- [29] M. Beneke and T. Feldmann, *Symmetry breaking corrections to heavy to light B meson form-factors at large recoil*, *Nucl. Phys. B* **592** (2001) 3 [[hep-ph/0008255](#)] [[INSPIRE](#)].
- [30] BELLE collaboration, *Search for $B^+ \rightarrow \ell^+ \nu_\ell \gamma$ decays with hadronic tagging using the full Belle data sample*, *Phys. Rev. D* **91** (2015) 112009 [[arXiv:1504.05831](#)] [[INSPIRE](#)].
- [31] BELLE collaboration, *Search for the rare decay of $B^+ \rightarrow \ell^+ \nu_\ell \gamma$ with improved hadronic tagging*, *Phys. Rev. D* **98** (2018) 112016 [[arXiv:1810.12976](#)] [[INSPIRE](#)].
- [32] A.M. Galda, M. Neubert and X. Wang, *Factorization and Sudakov resummation in leptonic radiative B decay — a reappraisal*, *JHEP* **07** (2022) 148 [[arXiv:2203.08202](#)] [[INSPIRE](#)].
- [33] M. Neubert, *Renormalization-group improved calculation of the $B \rightarrow X_s \gamma$ branching ratio*, *Eur. Phys. J. C* **40** (2005) 165 [[hep-ph/0408179](#)] [[INSPIRE](#)].